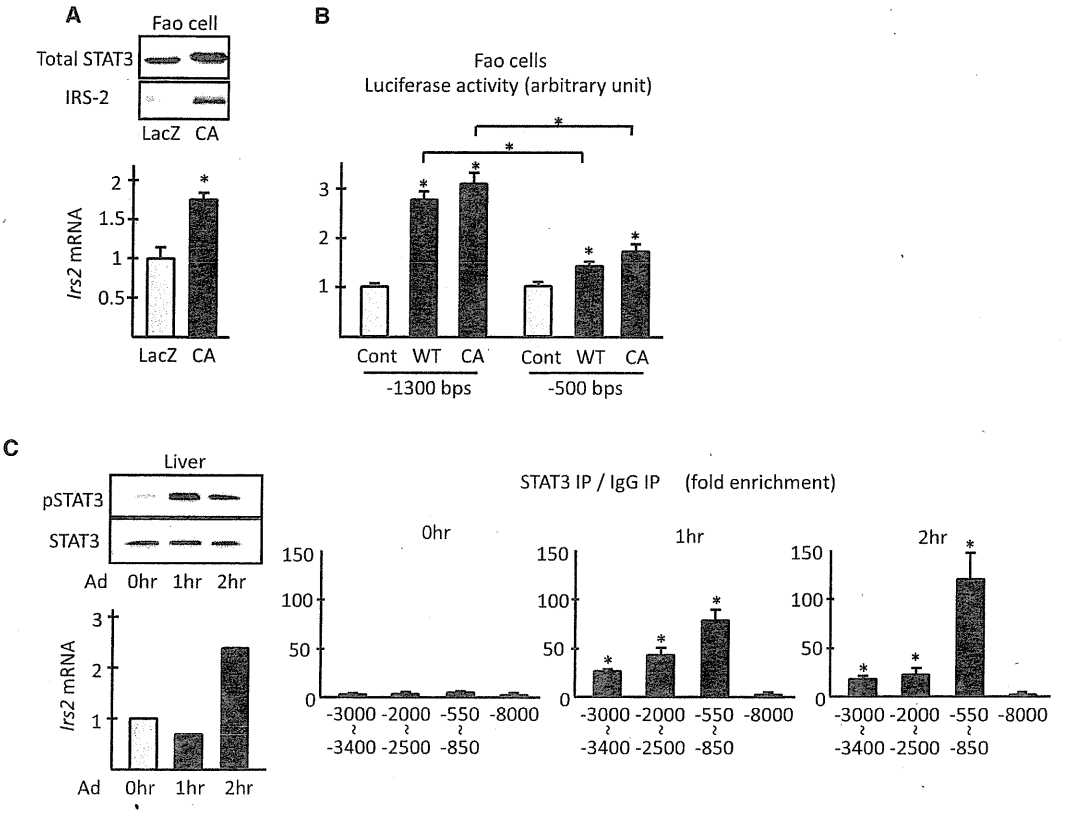

Figure 5. STAT3 Involvement in Hepatic IRS-2 Upregulation by Adiponectin

(A) Fao cells were infected with adenovirus encoding constitutively active STAT3 (CA) or LacZ. At 48 hr after infection, the cells were subjected to immunoprecipitation and immunoblotting with STAT3 and IRS-2 antibody, respectively. The total mRNA was subjected to RT-PCR analysis (n = 4, * $p < 0.05$).

(B) *Irs2* promoter activity in Fao cells. Fao cells transfected with the reporter vector harboring −1300 or −500 bp *Irs2* promoter were overexpressed with wild-type (WT) or CA STAT3. The cells were subjected to luciferase assay. The arbitrary units of luciferase activity are shown (n = 4, * $p < 0.05$).

(C) Chromatin immunoprecipitation of *Irs2* promoter regions with STAT3 antibody in liver. *db/db* mice were injected with adiponectin (Ad) at the fasted state, and the livers were removed at the indicated hours. The western blot of pSTAT3 and the mRNA expression of *Irs2* are shown in the left panels. The livers were immunoprecipitated with anti-STAT3 antibody, and −3000 to −3400, −2000 to −2500, and −550 to −850 of *Irs2* promoter region in the immunoprecipitated DNA was quantified by RT-PCR analysis. Fold enrichment compared to immunoprecipitation with control IgG antibody is shown (n = 3, * $p < 0.05$).

Error bars represent mean ± SEM.

with the −550 to −850 regions showing the highest enrichment (Figure 5C).

Adiponectin Induced IL-6 from Macrophages

We next investigated the origin of IL-6 induction by adiponectin. Fractionation experiments of the perigonadal WAT of adiponectin-treated *db/db* mice revealed that *Il6* mRNA was almost exclusively detected in the stromal vascular cell (SVC) fraction (Figure 6A). This finding was consistent with the immunohistochemistry analyses showing that IL-6 was exclusively costained with F4/80 in perigonadal WAT of adiponectin-treated *db/db* mice (Figure 6B). Indeed, adiponectin strongly upregulated *Il6* expression in cultured macrophages such as RAW264.7 cells or primary peritoneal macrophages, and not in fully differentiated 3T3L1 adipocytes (Figure 6C). We also conducted bone marrow transplantation (BMT) experiments, in which IL-6 KO mice were transplanted with BM from either IL-6 KO mice or wild-type mice. At 8 weeks after BMT, >99% of the leukocytes in peripheral blood were repopulated by donor cells (data not shown). IL-6 KO mice with the wild-type BM showed robust IL-6 induction by adiponectin and displayed significant *Irs2* upregulation in liver (Figure 6D), indicating that the IL-6 from BM-derived mononuclear cells was sufficient for IRS-2 induction by adiponectin. Importantly, adiponectin stimulation did not induce *Il6* in Fao cells (data not shown), indicating that the weak *Il6* mRNA induction observed in the livers of *db/db* mice or IL-6 KO mice transplanted with wild-type BM could be accounted for by non-hepatocyte cells, such as Kupffer cells or the resident macrophages in liver.

Adiponectin Induced IL-6 via NFκB Pathway in a Form-Dependent Manner, Independently of AdipoR1/AdipoR2

We further investigated the mechanism of IL-6 induction by adiponectin. Adiponectin-induced IL-6 production was associated with a decrease of IκBα, the inhibitory molecule of NFκB, in perigonadal WAT (Figure 7A). Indeed, ChIP assay with mouse peritoneal macrophages showed that immunoprecipitation with NFκB

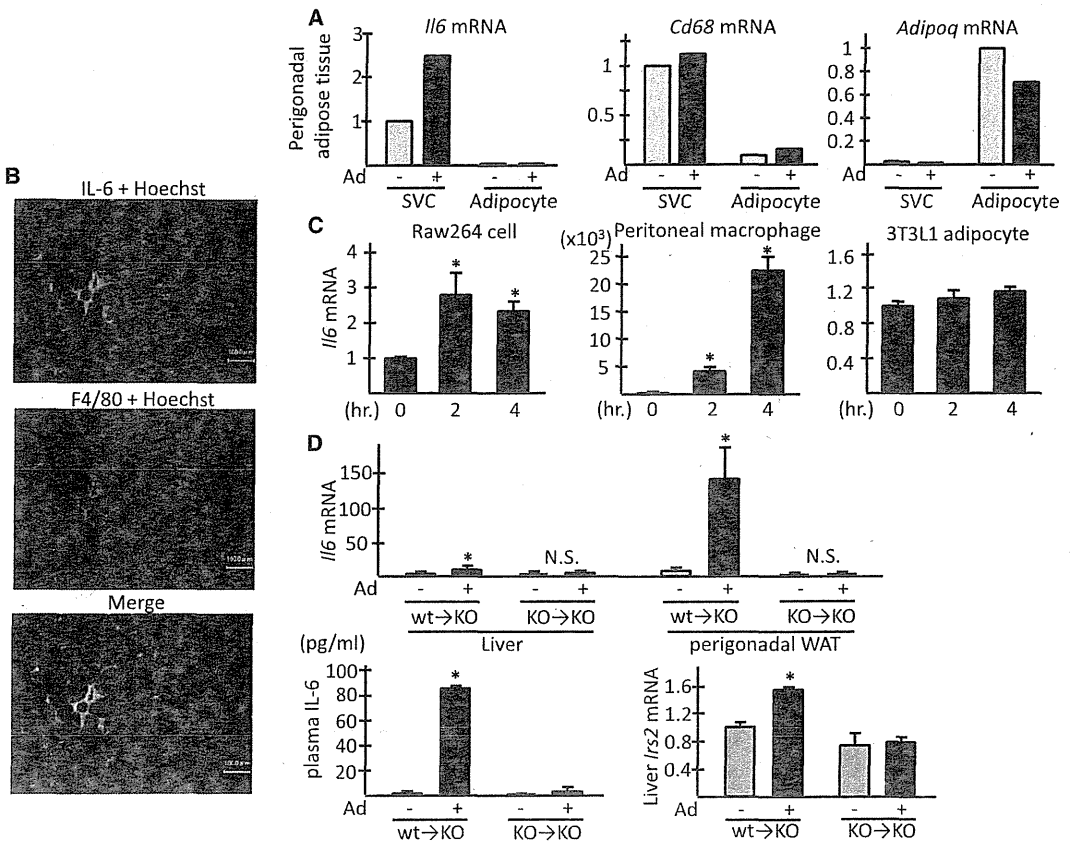

Figure 6. Upregulation of IL-6 by Adiponectin from Macrophages

(A) *Il6* expression in stromal vascular cells (SVCs) and adipocytes from perigonadal WAT of *db/db* mice injected with adiponectin. The *db/db* mice were injected with adiponectin (Ad) at the fasted state, and the perigonadal WAT was removed at 2 hr. SVCs and adipocytes were fractionated and subjected to mRNA extraction and RT-PCR analysis.

(B) IL-6 staining of perigonadal WAT after adiponectin administration. *db/db* mice were injected with Ad at the fasted state, and the perigonadal WAT was removed at 2 hr. The samples were subjected to immunostaining for F4/80 (red), IL-6 (green), and DNA (blue).

(C) RT-PCR analysis for *Il6* mRNA expression in RAW264.7 cells, primary peritoneal macrophages and fully differentiated 3T3L1 adipocytes after Ad stimulation ($n = 5$, $^* p < 0.05$).

(D) IL-6 induction and IRS-2 upregulation in IL-6 KO mice transplanted with bone marrow from wild-type C57BL/6J mice. The IL-6 KO mice transplanted with bone marrow from wild-type C57BL/6J mice (wt→KO) or IL-6 KO mice (KO→KO) were injected with Ad at the fasted state. The plasma was collected, and the liver and the perigonadal adipose tissues were removed at 2 hr. Plasma IL-6 concentration was determined by ELISA assay, and the total mRNA from the tissues was subjected to RT-PCR analysis ($n = 5–6$, $^* p < 0.05$).

Error bars represent mean ± SEM.

p65 subunit antibody significantly enriched the NFκB binding site of *Il6* promoter region (Libermann and Baltimore, 1990) after adiponectin stimulation (Figure 7B), suggesting that adiponectin induced IL-6 in macrophages through transcriptional regulation by NFκB.

Adiponectin exists in various forms in plasma such as trimer, hexamer, and high molecular weight (HMW), as well as a proteolytically cleaved form, globular adiponectin (Fruebis et al., 2001; Waki et al., 2005). It has been reported that the globular, trimer, and higher-molecular-weight forms of adiponectin activate AMPK via AdipoR1, whereas the HMW form also activates NFκB (Tsao et al., 2003). As nonreduced PAGE showed that the full-length adiponectin that we prepared contained trimer, hexamer, and higher-molecular-weight complexes (data not shown), it was unclear which form of adiponectin was responsible for IL-6 production in our study. In addition, adiponectin, which we prepared from *E. coli*, was inevitably contaminated with lipopolysaccharide (LPS), a strong inducer of IL-6 production, although the degree of LPS was as low as 1 pg/mg adiponectin after meticulous decontamination (data not shown). To address these issues, we stimulated RAW264.7 cells with various forms of adiponectin prepared from mammalian cells or *E. coli*. The results showed that the full-length adiponectin was the most potent, and the trimeric form was a less potent inducer of IL-6, whereas globular adiponectin did not induce IL-6 at all (Figure 7C). The form dependency was irrelevant to whether adiponectin was prepared from mammalian cells or *E. coli*.

Even more intriguingly, disruption of AdipoR1 and AdipoR2 (DKO) (Yamauchi et al., 2007) still showed robust upregulation

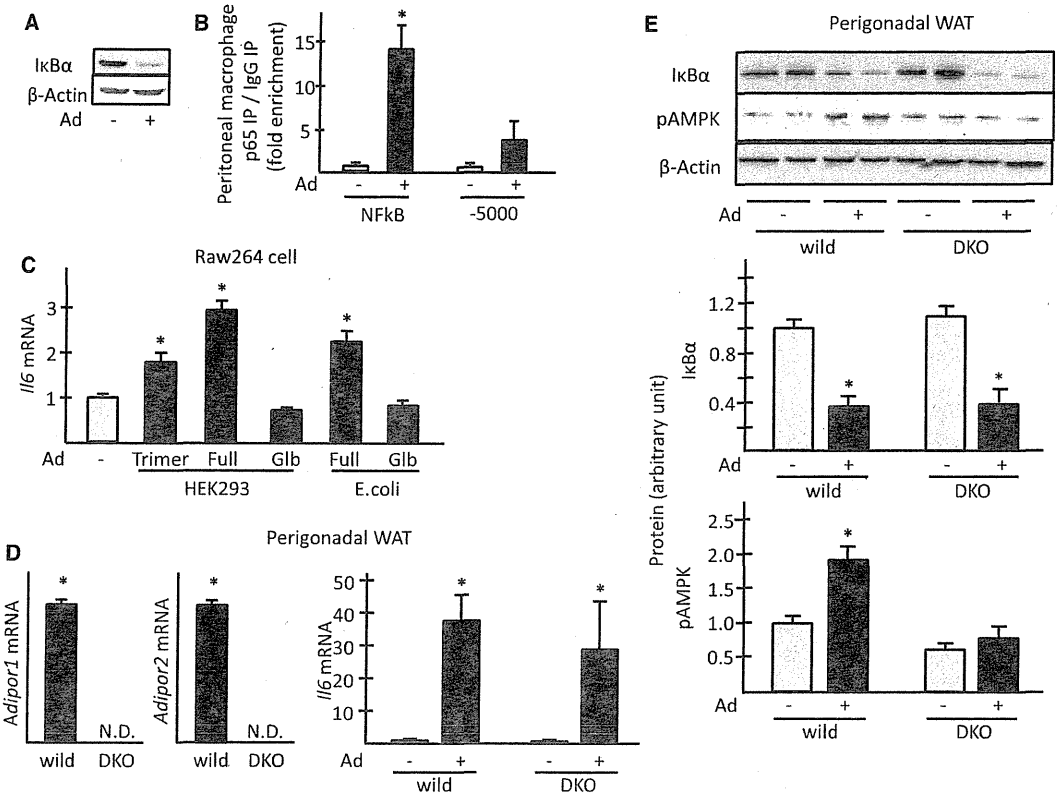

Figure 7. Upregulation of IL-6 via NFκB Pathway by Adiponectin in a Form-Dependent Manner Independently of Adiponectin Receptors

(A and B) Activation of NFκB pathway by adiponectin.

(A) The *db/db* mice were injected with adiponectin (Ad) at the fasted state, and the perigonadal WAT was removed at 2 hr. The total cell lysates were subjected to western blotting with the antibody for IκBα or β-actin.

(B) Chromatin immunoprecipitation of *Il6* promoter with the antibody for p65 subunit of NFκB. The mouse primary peritoneal macrophages were stimulated with Ad for 2 hr. The cells were immunoprecipitated with p65 antibody, and the precipitated DNA of NFκB binding site of *Il6* promoter was quantified by RT-PCR analysis. The −5000 region of the *Il6* promoter was used as the negative control. Fold enrichment compared to immunoprecipitation with control IgG antibody is shown (n = 3, *; $p < 0.05$).

(C) RT-PCR analysis of *Il6* mRNA in RAW264.7 cells stimulated with various forms of adiponectin (Ad). RAW264.7 cells were stimulated with 25 μg/ml trimeric form (Trimer), full-length (Full), or globular form (Glb) adiponectin prepared from HEK293 or *E. coli* for 2 hr. The total mRNA was subjected to RT-PCR analysis. (n = 4, * $p < 0.05$).

(D and E) IL-6 induction and IκBα degradation in perigonadal adipose tissues of AdipoR KO mice. The mice with targeted disruption of AdipoR1 and AdipoR2 (DKO) or their control mice were injected with Ad at the fasted state. The perigonadal WAT was removed at 2 hr and the total mRNA was subjected to RT-PCR analysis for *Adipor1*, *Adipor2* and *Il6* expression (n = 5, * $p < 0.05$; N.D., not detected) (D) or the total cell lysates were immunoblotted with IκBα, pAMPK and β-actin antibody (E). The arbitrary quantifications of immunoblots were shown in the lower panel (n = 3–5, * $p < 0.05$).

Error bars represent mean ± SEM. See also Figure S3.

of *Il6* by adiponectin in the perigonadal WAT (Figure 7D). The degradation of IκBα by adiponectin was also observed, while AMPK activation, the downstream molecule of AdipoR1, was abrogated (Figure 7E). As T-cadherin (*Cdh13*) mRNA was undetectable in RAW264.7 cells (data not shown), consistent with the previous report (Ivanov et al., 2001), these data suggest that there still exists an unidentified molecule in macrophages functioning as the receptor for hexamer or HMW adiponectin that mediates IL-6 upregulation.

DISCUSSION

In this study, we have discovered a pathway in which adiponectin upregulates IRS-2 in liver. The data also suggest the existence of an unidentified adiponectin receptor and indicate that the activation of STAT3 and subsequent increase in IRS-2 are mediated by IL-6 (Figure S3).

As previously reported, adiponectin activates AMPK, which suppresses gluconeogenic gene expressions (Yamauchi et al., 2002). Here, we propose that the IRS-2-mediated insulin-sensitization could be, besides AMPK activation, another mechanism whereby adiponectin exerts its antidiabetic actions. IRS-2 upregulation by adiponectin suppresses gluconeogenesis but does not enhance lipogenesis, consistent with our previous report showing that the suppression of SREBP1c is mediated largely via AMPK (Awazawa et al., 2009) and that IRS-2 mainly contributes to suppression of gluconeogenesis by insulin (Kubota et al., 2008).

IRS-1 and IRS-2 have partially overlapping but distinct functions in liver. Especially during the fasted state, IRS-2 increases and plays pivotal roles at its peak level immediately after refeeding (Kubota et al., 2008), while IRS-1 dominates during refeeding or in refed conditions (Guo et al., 2009). To date, several pathways have been identified to regulate IRS-2 expression, such as cAMP response element binding protein (CREB) and FoxO1 during fasting (Ide et al., 2004; Jhala et al., 2003; Shimomura et al., 2000) and SREBP1c after refeeding (Ide et al., 2004). Our findings suggest a mechanism of IRS-2 regulation via STAT3.

IL-6 activates STAT3 via IL-6 receptor/gp130 complex, while STAT3 is known to be phosphorylated by other cytokines (Levy and Darnell, 2002). Previous reports have suggested that the activation of gp130 interfacing with receptors other than the IL-6 receptor also contributes to STAT3 activation by IL-6 (Ernst et al., 2001). In our experiment, STAT3 phosphorylation reached its peak at 0.5–1 hr after IL-6 administration, whereas plasma IL-6 elevation and the maximal STAT3 phosphorylation concurrently occurred at 1–2 hr after adiponectin administration. Comparing the time course of these suggests that STAT3 activation induced by adiponectin is via the direct binding of IL-6 to the IL-6/gp130 receptor, although the possibility still remains that other ligand-receptor interactions are also involved.

Although IL-6 has usually been related to insulin resistance (Pradhan et al., 2001), some reports have paradoxically suggested that IL-6 contributes to improved insulin sensitivity (reviewed in Pedersen and Febbraio, 2008). Our data indicate that transient elevation of IL-6 levels leads to IRS-2 upregulation and enhances insulin signaling in liver. In contrast, in obese model mice, hepatic IRS-2 is downregulated in liver in spite of chronic plasma IL-6 elevation, possibly due to hyperinsulinemia. Even under these pathological conditions, the transient further increase in IL-6 levels accomplished by therapeutic administration of adiponectin leads to STAT3 phosphorylation and IRS-2 upregulation, suggesting that the acute change in IL-6 level, regardless of its absolute value, is critical for the subsequent STAT3 activation and IRS-2 upregulation. Indeed, transient IL-6 upregulation occurs in some physiologic circumstances such as muscle contraction, which is implicated in insulin sensitivity (Febbraio et al., 2004; Kelly et al., 2009). We have also found that in physiologic conditions IL-6 and adiponectin show similar diurnal variation in their expressions with their peaks in the fasting state, although the causal relations between these circadian changes and their physiological implications are not fully tested and need to be further validated. There is also still much debate as to whether chronically elevated IL-6 levels could actually contribute to systemic insulin resistance in obesity (Holmes et al., 2008; Torisu et al., 2007); this concept awaits future research.

We have shown by in vitro and BMT experiments that the macrophages mediate, and are sufficient for, the IL-6 induction and the resultant IRS-2 upregulation by adiponectin. Whereas IL-6 is known to be produced in adipocytes (Fain et al., 2004; Kershaw and Flier, 2004), our results consistently indicate that the IL-6 is mainly derived from SVCs, although the experiment using isolated SVCs could have a limitation due to the strong induction of IL-6 during the isolation process (Ruan et al., 2003). However, our data indicate that the *Il6* induction in liver by adiponectin originated in non-hepatocyte cells such as Kupffer cells, consistent with our previous report showing that AdipoR1/2 are the only functional receptors in hepatocytes (Yamauchi et al., 2007). We hypothesize that the unknown adiponectin receptor suggested here, which mediates *Il6* induction via the NFκB pathway, is expressed in macrophages but not in hepatocytes or adipocytes. This hypothesis explains the strong and specific IL-6 production in macrophages induced by adiponectin, although we could not completely rule out the possibility that other cells or tissues also contribute to IL-6 induction by adiponectin. The identification of the still unknown receptor in the future will resolve this issue and will also add depth to our knowledge about the field of metabolism by clarifying the significance of IRS-2 regulation as well as IL-6 induction by adiponectin in physiological or pathophysiological settings.

Previous reports indicate that adiponectin suppresses inflammatory responses induced by hyperglycemia (Devaraj et al., 2008) or TNF-α (Zhang et al., 2009), while others have reported that adiponectin by itself activates NFκB and promotes inflammatory cytokine production (Haugen and Drevon, 2007; Rovin and Song, 2006). The important aspect of this issue is that adiponectin could exert diverse effects upon inflammation and metabolism through different pathways. AMPK, as an anti-inflammatory molecule, is activated by various forms of adiponectin (Tsao et al., 2002), presumably via AipoR1, while NFκB has been shown to be activated by the HMW form (Tsao et al., 2003). As we have shown here, IL-6 is upregulated by adiponectin, whereas AMPK activation is totally abolished, in AdipoR1 and R2 knockout mice. T-cadherin, another possible receptor for hexameric and HMW forms of adiponectin in the cardiovascular system (Denzel et al., 2010; Hug et al., 2004), is undetectable in macrophages in vivo (Ivanov et al., 2001) and in RAW264.7 cells in our own study. These data indicate that there still exists an unidentified molecule in macrophages functioning as the receptor for hexamer or HMW adiponectin, and that adiponectin could exert distinct actions through different receptors in a context-dependent manner.

In conclusion, we have unraveled an insulin-sensitizing action initiated by adiponectin leading to upregulation of hepatic IRS-2 via a macrophage-derived IL-6-dependent pathway. Our data not only provide insight into adiponectin biology including the existence of a still unidentified adiponectin receptor, but also challenge the widely accepted idea about how IL-6/STAT3 signaling serves for systemic glucose metabolism, suggesting the possibility that recovery or creation of diurnal variations of adiponectin/IL-6 axis can be a therapeutic strategy for obesity-induced insulin resistance.

EXPERIMENTAL PROCEDURES

Reagents

Recombinant adiponectin was prepared as described previously (Yamauchi et al., 2002). Trimeric and full-length forms of adiponectin derived from HEK293 cells, and globular adiponectin derived from *E. coli* were purchased from ProSpec. Globular adiponectin derived from HEK293 cells was purchased from Alexis Biochemicals. Recombinant human IL-6 was purchased from R&D systems.

Animals

BKS.Cg-*m* +/+ *Lepr*^{db}/J (*db/db*) mice and C57BL/6J mice were purchased from Japan CLEA. C57BL/6J.129S6-*Il6*^{tm1Kopf} (IL-6 KO) mice were purchased

from Jackson laboratory. Generation of Ad KO mice and AdipoR-deficient mice were described previously (Kubota et al., 2002; Yamauchi et al., 2007). LST3KO mice were kindly provided by H. Inoue and M. Kasuga (Inoue et al., 2004). The mice were injected with 3 μg/g BW recombinant adiponectin intraperitoneally after overnight fasting at the age between 8 and 10 weeks. A total of 1 μg/g BW recombinant human IL-6 was injected to C57BL/6J mice (Cressman et al., 1996; Yamada et al., 1997). For western blotting, five units of insulin was injected into the inferior venae cavae of anesthetized mice, and the livers were removed after 5 min, except for western blotting of phospho-FoxO1, where the livers were removed after 2 min. The Animal Care Committee of the University of Tokyo approved the animal care and experimental procedures.

Immunoprecipitation and Immunoblotting

Immunoprecipitation and immunoblotting were conducted as previously described (Awazawa et al., 2009). The blood samples were collected from the mice after 24 hr fasting or 4 hr refeeding, and 1 μl plasma was subjected to adiponectin immunoblotting. 4G10, anti-IRS-1, anti-IRS-2, and anti-PI3-K p85 subunit N-SH2 antibodies were purchased from Millipore. Anti-insulin receptor antibody (C-19) and anti-gp130 antibody (C-20) were purchased from SantaCruz Biotechnology. Antibody for the p65 subunit of NFκB (ab7970) and adiponectin were purchased from Abcam. All the other antibodies were purchased from Cell Signaling Technology.

PI3 Kinase Assay

Five units of insulin was injected into the inferior venae cavae of anesthetized mice, and the livers were removed after 2 min. PI3 kinase activities in the liver was determined in immunoprecipitates with the indicated antibodies as previously described (Ueki et al., 2000). The phosphorylated lipids were visualized by autoradiography with an image analyzer (BAS 2000; Fuji Film, Tokyo).

Quantitative Real-Time PCR

The total RNA was prepared by RNeasy kit (QIAGEN). Complementary DNA was prepared by Reverse Transcription Reagents (Applied Biosystems). Quantitative real-time PCR was performed with ABI Prism with PCR Master Mix Reagent (Applied Biosystems) except for quantification of *Il6* mRNA in BMT experiment, where Power SYBR Green PCR Master Mix was used with the primers as follows: fwd, TTCCATCCAGTTGCCTTCTTGG; rev, TTCTCATTTC CACGATTTCCCAG. Levels of mRNA were normalized to that of cyclophilin (Awazawa et al., 2009). The other primers and probes were purchased from Applied Biosystems.

Cells and Cell Culture

RAW264.7 cells and fully differentiated 3T3L1 cells were cultured in DMEM (GIBCO) medium. Fao cells were cultured in RPMI1640 (GIBCO) medium. Primary peritoneal macrophages were isolated from 8-week-old male C57BL/6J mice injected with 3% thioglycollate. Isolation of adipocytes and SVCs was conducted as previously described (Kamei et al., 2006). All the media were supplemented with 10% (vol/vol) fetal bovine serum (GIBCO). Where indicated, the cells were infected with adenoviruses and harvested 48 hr after infection, and cells were stimulated with 25 μg/ml adiponectin.

Generation and Infection of Adenoviruses

Adenovirus of a constitutively active form of STAT3 was kindly provided by H. Inoue and M. Kasuga (Kobe University) (Inoue et al., 2004). Prior to use, all adenoviruses were purified on a cesium chloride gradient and dialyzed into PBS plus 10% glycerol. The cells were infected with the adenoviruses at the MOI (multiplicity of infection, or number of viral particles per cell) of 1000 PFU/cell.

IL-6 Neutralization

C57BL/6J mice were injected with 47 μg of anti-IL6 antibody or its isotype control (R&D Systems) via tail vein. The following day after overnight fasting, the mice were injected with 3 μg/g BW recombinant adiponectin intraperitoneally and sacrificed at 2 hr.

Luciferase Assay

Luciferase reporter plasmid harboring 5′-flanking region of mouse *Irs2* exon 1 was subcloned to pGL3 basic vector. Fao cells plated onto a 24-well plate were transfected with 0.5 μg of each luciferase reporter plasmid and 0.02 μg *Renilla* luciferase plasmid with HSV-TK promoter (phRL-TK, Promega) with Lipofectamine 2000 (Invitrogen). On the fourth day, the cells were harvested and the luciferase activity was measured by Dual-Luciferase Reporter Assay System (Promega) according to the manufacture's protocol.

Chromatin Immunoprecipitation Assay

ChIP assay was conducted as previously described (Friedman et al., 2004). In brief, mouse peritoneal macrophages or 1 g mouse liver was crosslinked in 1% formaldehyde/PBS. The tissue was suspended in lysis buffer (50 mM Tris-HCl [pH 8.1], 10 mM EDTA, 1% SDS, and protease inhibitor) and the chromatin was sheared by Bronson Sonifier 250D. The lysates were diluted five times with dilution buffer (16.7 mM Tris-HCl [pH 8.1], 167 mM NaCl, 1.2 mM EDTA, 0.01% SDS, 1.1% Triton X-100, and protease inhibitor). The chromatin solution was incubated with 2 μg primary antibodies and Dynabeads Protein A (Invitrogen). The beads were rinsed with wash buffer (50 mM HEPES-KOH [pH 7.0], 0.5 M LiCl, 1 mM EDTA, 0.7% sodium deoxycholate, and 1% NP-40) and immune complexes were eluted from beads with elution buffer (50 mM Tris-HCl [pH 8.0], 10 mM EDTA, 1% SDS) at 65 C°. Eluates were additionally incubated at 65C° to reverse crosslinking and then incubated with 0.5 mg/ml Proteinase K at 55 C°. DNA was purified with MinElute PCR purification kit (QIAGEN). The immunoprecipitated DNA regions were quantified by real time PCR using ABI Prism. (See also Table S1.)

Immunohistochemistry

The perigonadal fat pads were fixed in 4% paraformaldehyde in PBS and embedded in paraffin. The sections were incubated with rat F4/80 antibody (Serotec) (1:250 dilution) and goat IL-6 antibody (Santa Cruz) (1:50 dilution) at 4°C, followed by incubation with anti-rat IgG RITC (Santa Cruz) and anti-goat IgG FITC (Santa Cruz) for 1 hr at room temperature. Hoechst staining (1:400 dilution) was performed for 20 min at room temperature. The sections were mounted with Fluorescent Mounting Medium (DAKO) and examined under a fluorescence microscope (BZ-8000) (KEYENCE).

Analytical Procedures

Blood samples were collected by tail bleed. Plasma adiponectin and IL-6 concentrations were quantified by ELISA assay (Ohtuka Pharmaceuticals and R&D Systems, respectively).

Bone Marrow Transplantation

Bone marrow cells were collected by flushing of the femurs and tibiae of the mice at 6 weeks of age. The nucleated cells were counted and injected intravenously into lethally irradiated (10 Gy) male IL-6 KO mice at 6 weeks of age. The mice were maintained under normal chow diet for 8 weeks before experiments. For chimerism assay, the genomic DNA purified from the blood samples was subjected to Real-time PCR as previously described (Ichikawa et al., 2008).

Statistical Analysis

Statistical analysis was performed by two-sample t test assuming unequal variances or paired two-sample t test for means. Statistical significance was accepted at $p < 0.05$ unless otherwise indicated.

SUPPLEMENTAL INFORMATION

Supplemental Information includes Supplemental Experimental Procedures, three figures, and one table and can be found with this article online at doi:10.1016/j.cmet.2011.02.010.

ACKNOWLEDGMENTS

We thank F. Takahashi, Y. Kanto, R. Hoshino, and Y. Kishida for their excellent technical assistance. This work was supported by a grant for TSBMI from the Ministry of Education, Culture, Sports, Science and Technology of Japan (to T.K.), a Grant-in-aid for Scientific Research in Priority Areas (S) from the

Ministry of Education, Culture, Sports, Science, and Technology of Japan (to T.K.), a Grant-in-aid for Scientific Research from the Ministry of Health, Labor, and Welfare (to K.U.), Health Science Research grants (Research on Human Genome and Gene Therapy) from the Ministry of Health and Welfare (to T.K.), and a grant from Takeda Science Foundation (to K.U.).

Received: July 1, 2010
Revised: December 17, 2010
Accepted: February 3, 2011
Published: April 5, 2011

REFERENCES

Awazawa, M., Ueki, K., Inabe, K., Yamauchi, T., Kaneko, K., Okazaki, Y., Bardeesy, N., Ohnishi, S., Nagai, R., and Kadowaki, T. (2009). Adiponectin suppresses hepatic SREBP1c expression in an AdipoR1/LKB1/AMPK dependent pathway. Biochem. Biophys. Res. Commun. *382*, 51–56.

Berg, A.H., Combs, T.P., Du, X., Brownlee, M., and Scherer, P.E. (2001). The adipocyte-secreted protein Acrp30 enhances hepatic insulin action. Nat. Med. *7*, 947–953.

Cressman, D.E., Greenbaum, L.E., DeAngelis, R.A., Ciliberto, G., Furth, E.E., Poli, V., and Taub, R. (1996). Liver failure and defective hepatocyte regeneration in interleukin-6-deficient mice. Science *274*, 1379–1383.

Denzel, M.S., Scimia, M.-C., Zumstein, P.M., Walsh, K., Ruiz-Lozano, P., and Ranscht, B. (2010). T-cadherin is critical for adiponectin-mediated cardioprotection in mice. J. Clin. Invest. *120*, 4342–4352.

Devaraj, S., Torok, N., Dasu, M.R., Samols, D., and Jialal, I. (2008). Adiponectin decreases C-reactive protein synthesis and secretion from endothelial cells: evidence for an adipose tissue-vascular loop. Arterioscler. Thromb. Vasc. Biol. *28*, 1368–1374.

Dong, X., Park, S., Lin, X., Copps, K., Yi, X., and White, M.F. (2006). Irs1 and Irs2 signaling is essential for hepatic glucose homeostasis and systemic growth. J. Clin. Invest. *116*, 101–114.

Ernst, M., Inglese, M., Waring, P., Campbell, I.K., Bao, S., Clay, F.J., Alexander, W.S., Wicks, I.P., Tarlinton, D.M., Novak, U., et al. (2001). Defective gp130-mediated signal transducer and activator of transcription (STAT) signaling results in degenerative joint disease, gastrointestinal ulceration, and failure of uterine implantation. J. Exp. Med. *194*, 189–203.

Fain, J.N., Madan, A.K., Hiler, M.L., Cheema, P., and Bahouth, S.W. (2004). Comparison of the release of adipokines by adipose tissue, adipose tissue matrix, and adipocytes from visceral and subcutaneous abdominal adipose tissues of obese humans. Endocrinology *145*, 2273–2282.

Febbraio, M.A., Hiscock, N., Sacchetti, M., Fischer, C.P., and Pedersen, B.K. (2004). Interleukin-6 is a novel factor mediating glucose homeostasis during skeletal muscle contraction. Diabetes *53*, 1643–1648.

Friedman, J.R., Larris, B., Le, P.P., Peiris, T.H., Arsenlis, A., Schug, J., Tobias, J.W., Kaestner, K.H., and Greenbaum, L.E. (2004). Orthogonal analysis of C/EBPbeta targets in vivo during liver proliferation. Proc. Natl. Acad. Sci. USA *101*, 12986–12991.

Fruebis, J., Tsao, T.-S., Javorschi, S., Ebbets-Reed, D., Erickson, M.R.S., Yen, F.T., Bihain, B.E., and Lodish, H.F. (2001). Proteolytic cleavage product of 30-kDa adipocyte complement-related protein increases fatty acid oxidation in muscle and causes weight loss in mice. Proc. Natl. Acad. Sci. USA *98*, 2005–2010.

Guo, S., Copps, K.D., Dong, X., Park, S., Cheng, Z., Pocai, A., Rossetti, L., Sajan, M., Farese, R.V., and White, M.F. (2009). The Irs1 branch of the insulin signaling cascade plays a dominant role in hepatic nutrient homeostasis. Mol. Cell. Biol. *29*, 5070–5083.

Haugen, F., and Drevon, C.A. (2007). Activation of nuclear factor-kappaB by high molecular weight and globular adiponectin. Endocrinology *148*, 5478–5486.

Holmes, A.G., Mesa, J.L., Neill, B.A., Chung, J., Carey, A.L., Steinberg, G.R., Kemp, B.E., Southgate, R.J., Lancaster, G.I., Bruce, C.R., et al. (2008). Prolonged interleukin-6 administration enhances glucose tolerance and increases skeletal muscle PPARalpha and UCP2 expression in rats. J. Endocrinol. *198*, 367–374.

Hotamisligil, G.S., Peraldi, P., Budavari, A., Ellis, R., White, M.F., and Spiegelman, B.M. (1996). IRS-1-mediated inhibition of insulin receptor tyrosine kinase activity in TNF-alpha- and obesity-induced insulin resistance. Science *271*, 665–668.

Huang, H., Park, P.H., McMullen, M.R., and Nagy, L.E. (2008). Mechanisms for the anti-inflammatory effects of adiponectin in macrophages. J. Gastroenterol. Hepatol. *23* (*Suppl 1*), S50–S53.

Hug, C., Wang, J., Ahmad, N.S., Bogan, J.S., Tsao, T.-S., and Lodish, H.F. (2004). T-cadherin is a receptor for hexameric and high-molecular-weight forms of Acrp30/adiponectin. Proc. Natl. Acad. Sci. USA *101*, 10308–10313.

Ichikawa, M., Goyama, S., Asai, T., Kawazu, M., Nakagawa, M., Takeshita, M., Chiba, S., Ogawa, S., and Kurokawa, M. (2008). AML1/Runx1 negatively regulates quiescent hematopoietic stem cells in adult hematopoiesis. J. Immunol. *180*, 4402–4408.

Ide, T., Shimano, H., Yahagi, N., Matsuzaka, T., Nakakuki, M., Yamamoto, T., Nakagawa, Y., Takahashi, A., Suzuki, H., Sone, H., et al. (2004). SREBPs suppress IRS-2-mediated insulin signalling in the liver. Nat. Cell Biol. *6*, 351–357.

Inoue, H., Ogawa, W., Ozaki, M., Haga, S., Matsumoto, M., Furukawa, K., Hashimoto, N., Kido, Y., Mori, T., Sakaue, H., et al. (2004). Role of STAT-3 in regulation of hepatic gluconeogenic genes and carbohydrate metabolism in vivo. Nat. Med. *10*, 168–174.

Ivanov, D., Philippova, M., Antropova, J., Gubaeva, F., Iljinskaya, O., Tararak, E., Bochkov, V., Erne, P., Resink, T., and Tkachuk, V. (2001). Expression of cell adhesion molecule T-cadherin in the human vasculature. Histochem. Cell Biol. *115*, 231–242.

Iwabu, M., Yamauchi, T., Okada-Iwabu, M., Sato, K., Nakagawa, T., Funata, M., Yamaguchi, M., Namiki, S., Nakayama, R., Tabata, M., et al. (2010). Adiponectin and AdipoR1 regulate PGC-1alpha and mitochondria by Ca(2+) and AMPK/SIRT1. Nature *464*, 1313–1319.

Jhala, U.S., Canettieri, G., Screaton, R.A., Kulkarni, R.N., Krajewski, S., Reed, J., Walker, J., Lin, X., White, M., and Montminy, M. (2003). cAMP promotes pancreatic beta-cell survival via CREB-mediated induction of IRS2. Genes Dev. *17*, 1575–1580.

Kadowaki, T., Yamauchi, T., Kubota, N., Hara, K., Ueki, K., and Tobe, K. (2006). Adiponectin and adiponectin receptors in insulin resistance, diabetes, and the metabolic syndrome. J. Clin. Invest. *116*, 1784–1792.

Kamei, N., Tobe, K., Suzuki, R., Ohsugi, M., Watanabe, T., Kubota, N., Ohtsuka-Kowatari, N., Kumagai, K., Sakamoto, K., Kobayashi, M., et al. (2006). Overexpression of monocyte chemoattractant protein-1 in adipose tissues causes macrophage recruitment and insulin resistanc. J. Biol. Chem. *281*, 26602–26614.

Kelly, M., Gauthier, M.-S., Saha, A.K., and Ruderman, N.B. (2009). Activation of AMP-activated protein kinase by interleukin-6 in rat skeletal muscle: association with changes in cAMP, energy state, and endogenous fuel mobilization. Diabetes *58*, 1953–1960.

Kershaw, E.E., and Flier, J.S. (2004). Adipose tissue as an endocrine organ. J. Clin. Endocrinol. Metab. *89*, 2548–2556.

Kubota, N., Tobe, K., Terauchi, Y., Eto, K., Yamauchi, T., Suzuki, R., Tsubamoto, Y., Komeda, K., Nakano, R., Miki, H., et al. (2000). Disruption of insulin receptor substrate 2 causes type 2 diabetes because of liver insulin resistance and lack of compensatory beta-cell hyperplasia. Diabetes *49*, 1880–1889.

Kubota, N., Terauchi, Y., Yamauchi, T., Kubota, T., Moroi, M., Matsui, J., Eto, K., Yamashita, T., Kamon, J., Satoh, H., et al. (2002). Disruption of adiponectin causes insulin resistance and neointimal formation. J. Biol. Chem. *277*, 25863–25866.

Kubota, N., Kubota, T., Itoh, S., Kumagai, H., Kozono, H., Takamoto, I., Mineyama, T., Ogata, H., Tokuyama, K., Ohsugi, M., et al. (2008). Dynamic functional relay between insulin receptor substrate 1 and 2 in hepatic insulin signaling during fasting and feeding. Cell Metab. *8*, 49–64.

Levy, D.E., and Darnell, J.E., Jr. (2002). Stats: transcriptional control and biological impact. Nat. Rev. Mol. Cell Biol. *3*, 651–662.

Libermann, T.A., and Baltimore, D. (1990). Activation of interleukin-6 gene expression through the NF-kappa B transcription factor. Mol. Cell. Biol. *10*, 2327–2334.

Pedersen, B.K., and Febbraio, M.A. (2008). Muscle as an endocrine organ: focus on muscle-derived interleukin-6. Physiol. Rev. *88*, 1379–1406.

Pradhan, A.D., Manson, J.E., Rifai, N., Buring, J.E., and Ridker, P.M. (2001). C-reactive protein, interleukin 6, and risk of developing type 2 diabetes mellitus. JAMA *286*, 327–334.

Rovin, B.H., and Song, H. (2006). Chemokine induction by the adipocyte-derived cytokine adiponectin. Clin. Immunol. *120*, 99–105.

Ruan, H., Zarnowski, M.J., Cushman, S.W., and Lodish, H.F. (2003). Standard isolation of primary adipose cells from mouse epididymal fat pads induces inflammatory mediators and down-regulates adipocyte genes. J. Biol. Chem. *278*, 47585–47593.

Shimomura, I., Matsuda, M., Hammer, R.E., Bashmakov, Y., Brown, M.S., and Goldstein, J.L. (2000). Decreased IRS-2 and increased SREBP-1c lead to mixed insulin resistance and sensitivity in livers of lipodystrophic and ob/ob mice. Mol. Cell *6*, 77–86.

Sun, X.J., Wang, L.-M., Zhang, Y., Yenush, L., Myers, M.G., Jr., Glasheen, E., Lane, W.S., Pierce, J.H., and White, M.F. (1995). Role of IRS-2 in insulin and cytokine signalling. Nature *377*, 173–177.

Tamemoto, H., Kadowaki, T., Tobe, K., Yagi, T., Sakura, H., Hayakawa, T., Terauchi, Y., Ueki, K., Kaburagi, Y., Satoh, S., et al. (1994). Insulin resistance and growth retardation in mice lacking insulin receptor substrate-1. Nature *372*, 182–186.

Taniguchi, C.M., Emanuelli, B., and Kahn, C.R. (2006). Critical nodes in signalling pathways: insights into insulin action. Nat. Rev. Mol. Cell Biol. *7*, 85–96.

Torisu, T., Sato, N., Yoshiga, D., Kobayashi, T., Yoshioka, T., Mori, H., Iida, M., and Yoshimura, A. (2007). The dual function of hepatic SOCS3 in insulin resistance in vivo. Genes Cells *12*, 143–154.

Tsao, T.-S., Murrey, H.E., Hug, C., Lee, D.H., and Lodish, H.F. (2002). Oligomerization state-dependent activation of NF-kappa B signaling pathway by adipocyte complement-related protein of 30 kDa (Acrp30). J. Biol. Chem. *277*, 29359–29362.

Tsao, T.-S., Tomas, E., Murrey, H.E., Hug, C., Lee, D.H., Ruderman, N.B., Heuser, J.E., and Lodish, H.F. (2003). Role of disulfide bonds in Acrp30/adiponectin structure and signaling specificity. Different oligomers activate different signal transduction pathways. J. Biol. Chem. *278*, 50810–50817.

Ueki, K., Algenstaedt, P., Mauvais-Jarvis, F., and Kahn, C.R. (2000). Positive and negative regulation of phosphoinositide 3-kinase-dependent signaling pathways by three different gene products of the p85alpha regulatory subunit. Mol. Cell. Biol. *20*, 8035–8046.

Waki, H., Yamauchi, T., Kamon, J., Kita, S., Ito, Y., Hada, Y., Uchida, S., Tsuchida, A., Takekawa, S., and Kadowaki, T. (2005). Generation of globular fragment of adiponectin by leukocyte elastase secreted by monocytic cell line THP-1. Endocrinology *146*, 790–796.

Yamada, Y., Kirillova, I., Peschon, J.J., and Fausto, N. (1997). Initiation of liver growth by tumor necrosis factor: deficient liver regeneration in mice lacking type I tumor necrosis factor receptor. Proc. Natl. Acad. Sci. USA *94*, 1441–1446.

Yamauchi, T., Kamon, J., Waki, H., Terauchi, Y., Kubota, N., Hara, K., Mori, Y., Ide, T., Murakami, K., Tsuboyama-Kasaoka, N., et al. (2001). The fat-derived hormone adiponectin reverses insulin resistance associated with both lipoatrophy and obesity. Nat. Med. *7*, 941–946.

Yamauchi, T., Kamon, J., Minokoshi, Y., Ito, Y., Waki, H., Uchida, S., Yamashita, S., Noda, M., Kita, S., Ueki, K., et al. (2002). Adiponectin stimulates glucose utilization and fatty-acid oxidation by activating AMP-activated protein kinase. Nat. Med. *8*, 1288–1295.

Yamauchi, T., Kamon, J., Ito, Y., Tsuchida, A., Yokomizo, T., Kita, S., Sugiyama, T., Miyagishi, M., Hara, K., Tsunoda, M., et al. (2003). Cloning of adiponectin receptors that mediate antidiabetic metabolic effects. Nature *423*, 762–769.

Yamauchi, T., Nio, Y., Maki, T., Kobayashi, M., Takazawa, T., Iwabu, M., Okada-Iwabu, M., Kawamoto, S., Kubota, N., Kubota, T., et al. (2007). Targeted disruption of AdipoR1 and AdipoR2 causes abrogation of adiponectin binding and metabolic actions. Nat. Med. *13*, 332–339.

Zhang, P., Wang, Y., Fan, Y., Tang, Z., and Wang, N. (2009). Overexpression of adiponectin receptors potentiates the antiinflammatory action of subeffective dose of globular adiponectin in vascular endothelial cells. Arterioscler. Thromb. Vasc. Biol. *29*, 67–74.

Cell Metabolism

Thiazolidinediones Enhance Sodium-Coupled Bicarbonate Absorption from Renal Proximal Tubules via PPARγ-Dependent Nongenomic Signaling

Yoko Endo,[1] Masashi Suzuki,[1] Hideomi Yamada,[1] Shoko Horita,[1] Motoei Kunimi,[1] Osamu Yamazaki,[1] Ayumi Shirai,[1] Motonobu Nakamura,[1] Naoyuki Iso-O,[1] Yuehong Li,[1,3] Masumi Hara,[1] Kazuhisa Tsukamoto,[1] Nobuo Moriyama,[4] Akihiko Kudo,[5] Hayato Kawakami,[5] Toshimasa Yamauchi,[1] Naoto Kubota,[1] Takashi Kadowaki,[1] Haruki Kume,[2] Yutaka Enomoto,[2] Yukio Homma,[2] George Seki,[1,*] and Toshiro Fujita[1]

[1]Department of Internal Medicine
[2]Department of Urology, Faculty of Medicine
University of Tokyo, 7-3-1 Bunkyo-ku, Hongo, Tokyo 113-0033, Japan
[3]Department of Nephrology, People's Hospital, Peking University, 11 Xizhimen South Street, Beijing 100044, China
[4]Department of Experimental Nursing, Faculty of Nursing, Fukuoka Prefectural University, Tagawa-shi, Ida 4395, Fukuoka 825-8585, Japan
[5]Department of Anatomy, Kyorin University School of Medicine, 6-20-2 Shinkawa, Mitaka, Tokyo 181-8611, Japan
*Correspondence: georgeseki-tky@umin.ac.jp
DOI 10.1016/j.cmet.2011.02.015

SUMMARY

Thiazolidinediones (TZDs) improve insulin resistance by activating a nuclear hormone receptor, peroxisome proliferator-activated receptor γ (PPARγ). However, the use of TZDs is associated with plasma volume expansion through a mechanism that remains to be clarified. Here we showed that TZDs rapidly stimulate sodium-coupled bicarbonate absorption from the renal proximal tubule in vitro and in vivo. TZD-induced transport stimulation is dependent on PPARγ-Src-EGFR-ERK and observed in rat, rabbit and human, but not in mouse proximal tubules where Src-EGFR is constitutively activated. The existence of PPARγ-Src-dependent nongenomic signaling, which requires the ligand-binding ability, but not the transcriptional activity of PPARγ, is confirmed in mouse embryonic fibroblast cells. The enhancement of the association between PPARγ and Src by TZDs supports an indispensable role of Src in this signaling. These results suggest that the PPARγ-dependent nongenomic stimulation of renal proximal transport is also involved in TZD-induced volume expansion.

INTRODUCTION

Peroxisome proliferator-activated receptor γ (PPARγ) is a ligand-activated transcription factor that belongs to the nuclear hormone receptor gene superfamily (Yki-Järvinen, 2004). Pharmacological activation of PPARγ by thiazolidinediones (TZDs) such as rosiglitazone (RGZ) and pioglitazone (PGZ) significantly improves insulin resistance and lowers plasma glucose concentrations (Yki-Järvinen, 2004). TZDs may also have beneficial effects on the cardiovascular system, including the reduction of blood pressure and the improvement of vascular function (Ryan et al., 2004). However, fluid retention, one of the main side effects of TZDs, precludes the use of TZDs in the setting of severe heart failure (Mudaliar et al., 2003).

While the enhancement of sodium and fluid reabsorption from the kidney, in addition to the peripheral vasodilatation, may contribute to TZD-induced edema formation, the molecular mechanism underlying the renal tubular actions of TZDs has been a matter of controversy. Thus, the studies on mice with the selective deletion of PPARγ from renal collecting ducts originally suggested that TZD-induced volume expansion is dependent on transport stimulation in the distal nephrons (Guan et al., 2005; Zhang et al., 2005). In particular, the PPARγ-mediated enhanced transcription of the epithelial Na channel (ENaC) γ subunit was thought to play a key role (Guan et al., 2005; Zhang et al., 2005). TZDs might also enhance the surface expression of ENaC α subunit through the glucocorticoid-inducible kinase SGK1 (Hong et al., 2003). However, other studies did not support a central role of the ENaC in TZD-induced fluid retention. For example, TZDs did not alter basal and insulin-stimulated ENaC activities in well-established renal principal cell culture models (Nofziger et al., 2005). In addition, TZDs did not consistently enhance the expression of ENaC subunits (Song et al., 2004). While an ENaC inhibitor, amiloride, prevented TZD-induced volume expansion in mice (Guan et al., 2005), it failed to prevent volume expansion in rats induced by a non-TZD PPARγ agonist, GI262570 (Chen et al., 2005). Furthermore, TZD-induced fluid retention was not suppressed in mice lacking ENaC α subunit selectively in collecting ducts (Vallon et al., 2009), strongly suggesting that the enhancement of ENaC activity alone cannot explain TZD-induced volume expansion. On the other hand, both human (Zanchi et al., 2004) and animal (Muto et al., 2001) studies suggested that renal proximal tubule (PT) transport could be stimulated by TZDs. We reasoned that TZD-induced volume expansion is multifactorial and that PTs may be another target nephron segment of TZDs.

In the present study we demonstrate that TZDs markedly stimulate in vitro and in vivo PT transport. This rapid transport stimulation is dependent on PPARγ-Src-EGFR-ERK and observed in isolated PTs from rabbit, rat, and human. In mouse

PTs, however, TZDs fail to induce transport stimulation probably because of the unique constitutive activity of Src. The existence of PPARγ-Src-dependent nongenomic signaling, which requires the ligand-binding ability, but not the transcriptional activity, of PPARγ is confirmed in mouse embryonic fibroblast (EF) cells. Furthermore, TZDs rapidly enhance the association between PPARγ and Src, supporting an indispensable role of Src in this signaling. We propose that, in addition to enhanced expression of sodium transporter(s) through the PPARγ-dependent genomic signaling, the stimulation of renal PT transport through the PPARγ-dependent nongenomic signaling is also involved in TZD-induced volume expansion.

RESULTS

Effects of TZDs on Transport Functions in Isolated Rabbit PTs

To examine whether TZDs can stimulate PT transport, we first focused on the acute effects of TZDs on the electrogenic Na^+-HCO_3^- cotransporter NBCe1 that mediates the majority of Na^+-coupled HCO_3^- absorption from PTs (Li et al., 2008). In isolated luminally collapsed rabbit PTs, 0.3 μM PGZ markedly stimulated the NBCe1 activity within minutes (Figure 1A). Both PGZ and RGZ stimulated the NBCe1 activity at submicromolar, but not micromolar concentrations (Figures 1B and 1C). We next examined the effects of TZDs on the activity of luminal Na^+/H^+ exchanger NHE3 in luminally perfused PTs and found that 0.3 μM PGZ markedly stimulated the NHE3 activity (Figures S1A and S1B, available online). Submicromolar concentrations of PGZ also enhanced the rate of HCO_3^- absorption ($JHCO_3^-$) within 5 min (Figure 1D), indicating that TZDs can acutely stimulate the net Na^+ and HCO_3^- absorption from PTs by enhancing the activities of both NBCe1 and NHE3.

To examine the signaling mechanism of TZD-induced stimulation of PT transport, we used a tyrosine kinase inhibitor, genistein (20 μM), a MEK inhibitor, PD98059 (10 μM), a PPARγ antagonist, GW9662 (5 μM), an EGFR tyrosine kinase inhibitor, AG1478 (20 μM), a PKC inhibitor, calphostin C (0.5 μM), and a PKA inhibitor, H89 (10 μM). All of these inhibitors did not change the basal $JHCO_3^-$ values at the concentrations used in this study. While genistein, PD98059, GW9662, and AG1478 largely suppressed the PGZ-induced stimulation of $JHCO_3^-$, calphostin C and H89 were without effects (Figure 1E). PGZ also rapidly stimulated ERK phosphorylation in renal cortex tissues that was abolished by AG1478, GW9662, and PD98059 (Figure 1F). These results indicate that, among multiple rapid signaling pathways that are potentially activated by TZDs (Burgermeister and Seger, 2008), the EGFR/ERK pathway is critically involved in the effects of TZDs on PT transport. To confirm the involvement of PPARγ in TZD-induced PT transport stimulation, we performed immunohistochemical analysis on rabbit kidneys. In addition to the intense PPARγ expression in inner medullary collecting ducts as reported (Guan et al., 1997), the diffuse cytosolic expression of PPARγ in PTs was also evident (Figure 1G). Western blot analysis confirmed the expression of PPARγ protein in both medulla and cortex (Figure 1H). Together with the suppression of TZD-induced PT transport stimulation by GW9662, these results support a view that PPARγ-dependent signaling is involved in the TZD-induced stimulation of PT transport. The specificity of mouse and rabbit anti-PPARγ antibodies is shown in Figure S1C.

Species Differences in TZD's Effects on PT Transport

In view of potential species differences in the mechanism of TZD-induced fluid retention (Chen et al., 2005; Guan et al., 2005), we next examined the effects of TZDs on PT transport in the different species. PGZ at 0.3 μM stimulated NBCe1 activity in rats to a similar extent as in rabbits. However, the stimulatory effect of PGZ was absent in mice (Figure 2A). In mouse PTs, PGZ at concentrations from 0.003 to 3 μM failed to stimulate $JHCO_3^-$ (Figure 2B). Because both rat and mouse PTs express PPARγ (Figures 2C and 2D), the lack of transport stimulation by TZDs in mouse PTs cannot be attributable to the absence of PPARγ.

On the other hand, an Src inhibitor, PP2 (3 μM), completely suppressed the stimulatory effect of PGZ on NBCe1 activity in rabbit PTs (Figure 2E), consistent with the involvement of Src in TZD-induced stimulation of PT transport. Interestingly, mouse PTs were reported to have the unique constitutive activity of Src, which was not found either in other mouse tissues or in PTs of other species (Kiley and Chevalier, 2007). We hypothesized that the constitutive activation of Src, together with the dysregulation of downstream EGFR signaling (Kiley and Chevalier, 2007), might be responsible for the lack of stimulatory effect of TZDs in mouse PTs. Although PGZ stimulated renal cortex Src phosphorylation in rabbits and rats, it failed to induce Src phosphorylation in mice, presumably because of the highly phosphorylated basal status (Figure 2F). PGZ also stimulated ERK phosphorylation in rats, but not in mice because of the basal activation (Figure 2G). These results suggest that the constitutive activation of Src, which abolishes the estrogen receptor (ER)-mediated nongenomic activation of endothelial NO synthase (eNOS) (Li et al., 2007), also interferes with the PPARγ-mediated nongenomic signaling. In rat renal cortex, the PGZ-induced Src phosphorylation was suppressed by PP2, but not by AG1478. On the other hand, the PGZ-induced EGFR phosphorylation was suppressed by both PP2 and AG1478 (Figure S2). These results indicate that Src acts upstream of EGFR in the TZD-induced signaling.

Notably, human PTs do not have the constitutive activation of Src (Kiley and Chevalier, 2007) and hence may be sensitive to the stimulatory effect of TZDs. Indeed, 0.3 μM PGZ markedly stimulated the NBCe1 activity in isolated human PTs, and this stimulation was totally suppressed by PD98059 and GW9662 (Figure 3A). Immunohistochemical analysis revealed that PPARγ was diffusely expressed in human PTs (Figure 3B). Furthermore, western blot analysis confirmed the expression of PPARγ protein in isolated human PTs (Figure 3C).

Acute In Vivo Effects of TZDs

To examine whether the TZD-induced stimulation of PT transport modifies whole-body volume homeostasis, we performed acute clearance studies in water-loaded conscious rats. Rats were orally given PGZ at a single dose of 10 mg/kg body weight (BW) and urine was collected for over 90 min. Taking account of the high affinity of PGZ to plasma proteins, this protocol is estimated to keep the protein-unbound, plasma PGZ concentration at around 0.3 μM for at least 2 hr (Krieter et al., 1994). PGZ

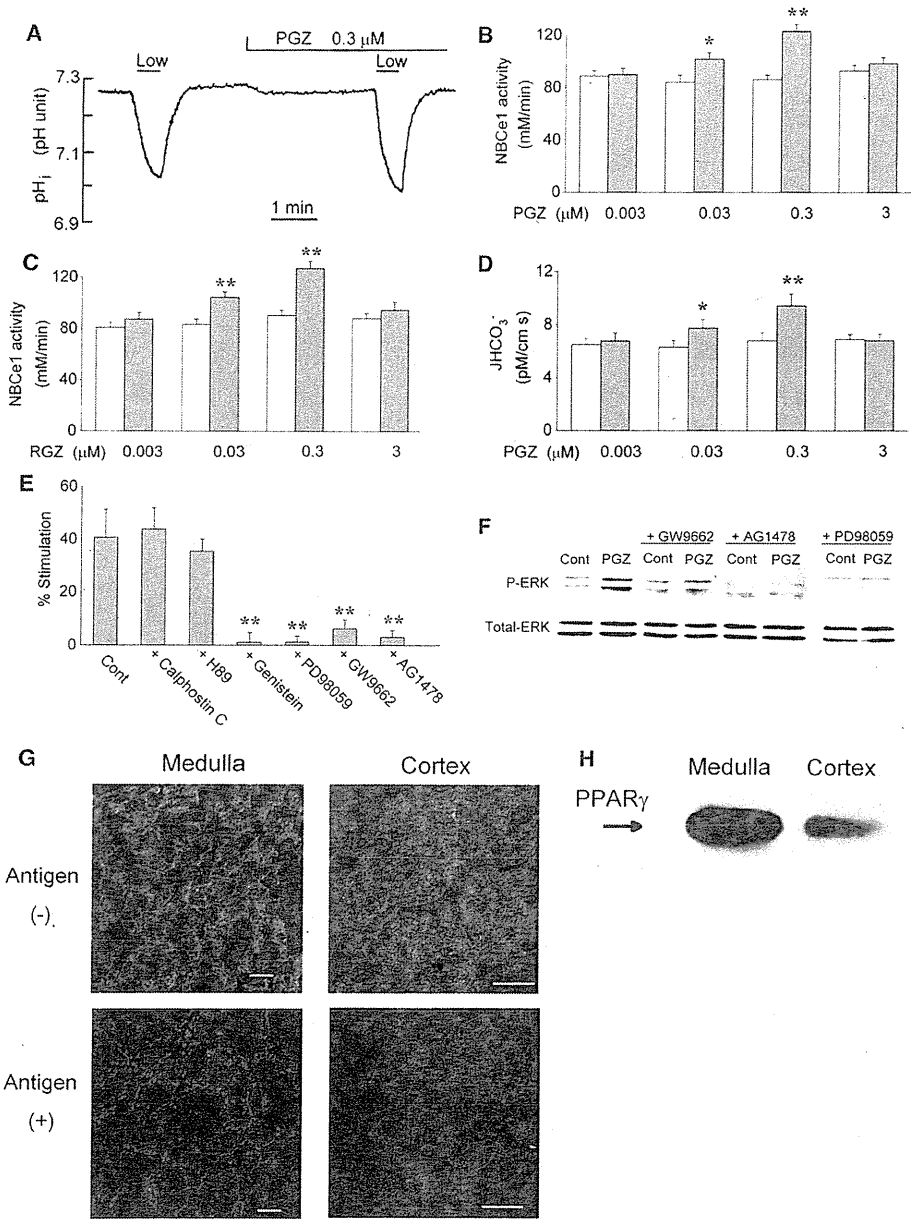

Figure 1. Stimulation of PT Transport by TZDs through PPARγ-Dependent Pathway in Rabbits

(A) pH_i responses to bath HCO_3^- reduction from 25 to 12.5 mM (indicated as Low) in isolated rabbit PT.

(B) Concentration dependency of PGZ effects on NBCe1 activity. Open bars represent the control activities and closed bars represent the activities 5 min after the addition of PGZ. *$p < 0.05$ versus control; **$p < 0.01$ versus control. Data are means ± SEM. Each n = 7.

(C) Concentration dependency of RGZ effects on NBCe1 activity. **$p < 0.01$ versus control. Data are means ± SEM. Each n = 7.

(D) Concentration dependency of PGZ effects on the rate of $JHCO_3^-$. Open bars represent the control fluxes and closed bars represent the fluxes 5 min after the addition of PGZ. *$p < 0.05$ versus control; **$p < 0.01$ versus control. Data are means ± SEM. Each n = 7.

(E) Roles of protein kinases and PPARγ in the stimulation of $JHCO_3^-$ by PGZ. Tubules were incubated with these inhibitors for 20 min. **$p < 0.01$ versus control. Data are means ± SEM of six to eight experiments.

(F) ERK phosphorylation in rabbit renal cortex tissues. The samples were incubated for 40 min in the absence or presence of inhibitors and 0.3 μM PGZ was added for 5 min. Total ERK and P-ERK were detected.

(G) Immunohistochemical analysis of PPARγ expression in rabbit kidney. The goat anti-PPARγ antibody was applied in the absence or presence of antigen (10 mg/L). Images are shown in pseudocolor, where green shows PPARγ, red shows actin, and blue shows nuclei. Bars = 50 μm.

(H) Western blot analysis on rabbit kidney with the mouse anti-PPARγ antibody. Each lane contained 20 μg of protein. See also Figure S1.

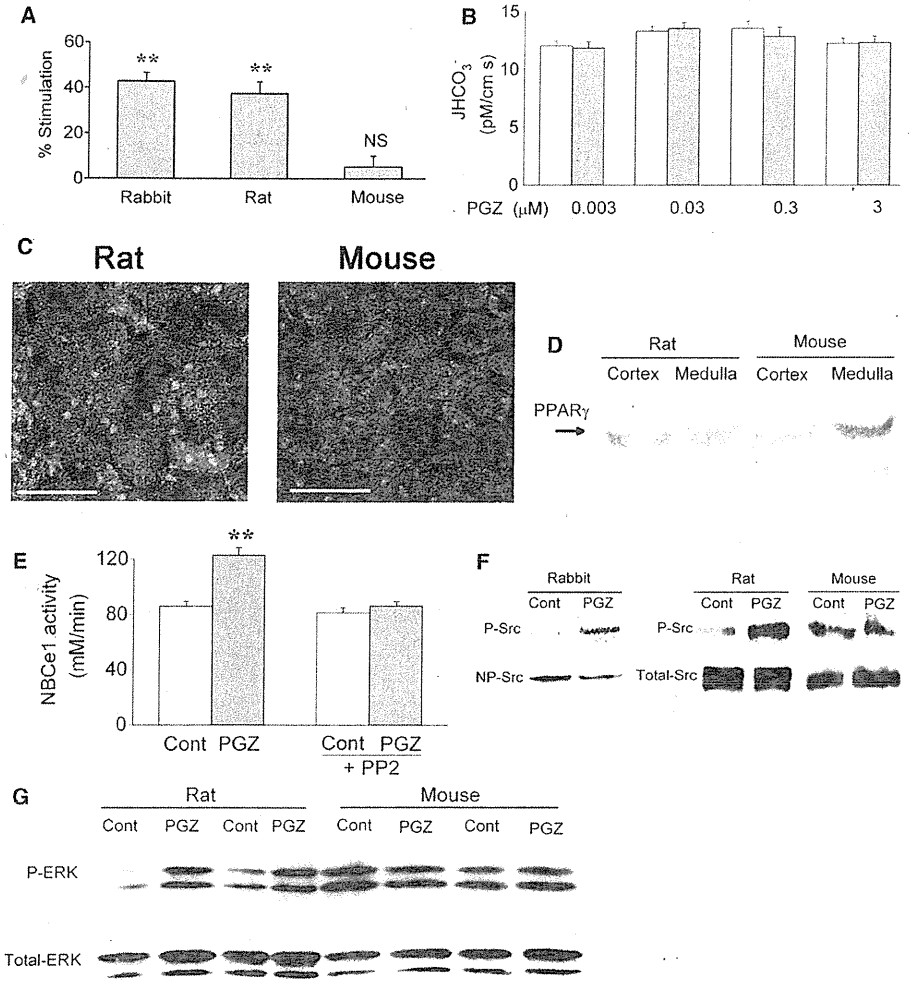

Figure 2. Species Difference in Effects of TZDs on PT Transport

(A) Effects of 0.3 μM PGZ on NBCe1 activity in rabbit, rat, or mouse. **$p < 0.01$ versus control. Data are means ± SEM of seven to eight experiments. NS, not significant.

(B) Concentration dependency of PGZ effects on $JHCO_3^-$ in mouse. Open bars represent the control fluxes and closed bars represent the fluxes 5 min after the addition of PGZ. Data are means ± SEM. Each n = 6.

(C) Immunohistochemical analysis of PPARγ expression in rat and mouse kidneys. Details are as in Figure 1G, but the rabbit anti-PPARγ antibody was used. Bars = 50 μm.

(D) Western blot analysis on rat and mouse kidneys with the rabbit anti-PPARγ antibody. Each lane contained 20 μg of protein.

(E) Effects of 0.3 μM PGZ on NBCe1 activity in isolated rabbit PTs in the absence and presence of Src inhibitor PP2 (3 μM). Open bars represent the control activities and closed bars represent the activities 5 min after the addition of PGZ. **$p < 0.01$ versus control. Data are means ± SEM. Each n = 7.

(F) Src phosphorylation in renal cortex tissues. The samples were treated with 0.3 μM PGZ for 5 min. Total Src, nonphosphorylated Src (NP-Src), and phosphorylated Src (P-Src) were detected.

(G) ERK phosphorylation in rat and mouse renal cortex tissues. Details are as in Figure 1F. See also Figure S2.

significantly reduced urinary volume (UV), fractional excretion of lithium ($FELi^+$), and free water clearance (CH_2O) without changing creatinine clearance (CCr) or urinary sodium excretion (UNaV) (Figure 4A). PGZ also slightly increased urinary osmolality (Uosm), which could be explained by the stimulation of PT absorption and the resultant decrease in delivery of water and electrolytes to the loop of Henle (de Rouffignac et al., 1991). Consistent with this interpretation, the simultaneous administration of a PT transport inhibitor, acetazolamide (ACZ), with PGZ abolished the changes in UV, $FELi^+$, CH_2O, and Uosm. Systolic blood pressure, analyzed by tail-cuff measurement, was unaffected by PGZ (Figure S3A). Mild sodium depletion during the acute clearance studies seemed to be responsible for the lack of PGZ effect on UNaV. Indeed, PGZ significantly reduced UV, $FELi^+$, CH_2O, as well as UNaV, and increased Uosm when rats were loaded with half saline (0.45% NaCl) instead of water

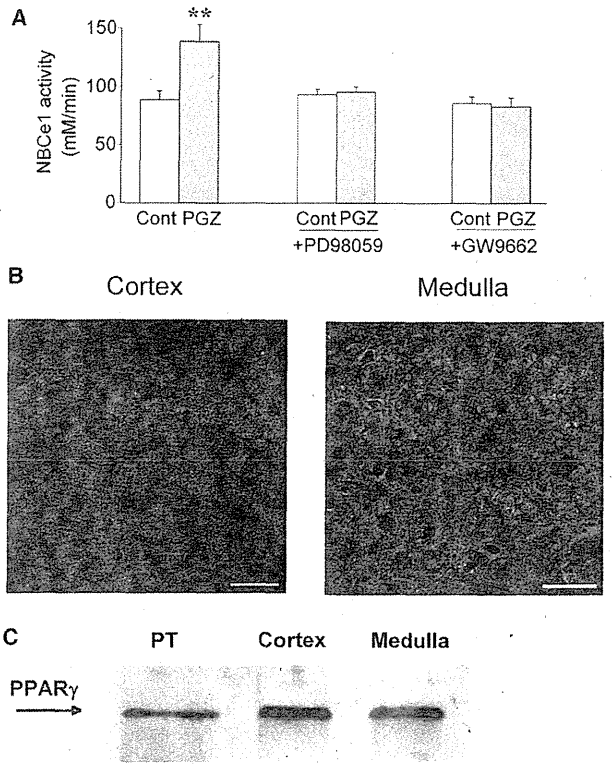

Figure 3. Effects of PGZ on Human PTs

(A) Effects of 0.3 μM PGZ on NBCe1 activity in isolated human PTs. Open bars represent the control activities and closed bars represent the activities 5 min after the addition of PGZ. **$p < 0.01$ versus control. Data are means ± SEM of six to eight experiments.

(B) Immunohistochemical analysis of PPARγ expression in human kidney. Details are as in Figure 1G, but the rabbit anti-PPARγ antibody was used. Bars = 50 μm.

(C) Western blot analysis on human kidney with the rabbit anti-PPARγ antibody. The left lane contained 30 PTs manually dissected from cortex slices and the middle and right lanes each contained 20 μg of proteins.

(Figure S3B). Immunohistochemical analysis revealed that the in vivo administration of PGZ enhanced ERK phosphorylation in in situ PTs (Figure 4B), which was confirmed by western blot analysis on renal cortex samples (Figure 4C). These results indicate that TZDs can acutely induce fluid retention by stimulating in vivo PT reabsorption in rats through the ERK-dependent pathway. On the other hand, the chronic RGZ administration for 3 days in rats was reported to enhance the expression of collecting duct water channel protein AQP2 (Song et al., 2004). However, we confirmed that the acute administration of PGZ did not affect the expression of AQP2 in renal medulla (Figure 4D).

We also performed acute clearance studies in mice with the identical water-loading protocol ($n = 11$ for both control and PGZ). Consistent with the lack of transport stimulation in isolated mouse PT, the acute administration of PGZ did not reduce UV (control, 3.8 ± 0.5 μl/10 g BW/min versus PGZ, 4.2 ± 0.4 μl/10 g BW/min), $FELi^+$ (control, 19.1 ± 2.4% versus PGZ, 21.8 ± 4.0%) or CH_2O (control, 0.62 ± 0.18 μl/10 g BW/min versus PGZ, 0.80 ± 0.25 μl/10 g BW/min) in mice.

PPARγ-Dependent Stimulation of NHE1 Activity in EF Cells

To further examine the nature of the PPARγ-dependent rapid signaling pathway, we took advantage of EF cells, the only viable cells available from $PPAR\gamma^{-/-}$ mice (Kubota et al., 1999) and focused on the regulation of NHE1, the ubiquitously expressed Na^+/H^+ exchanger that is rapidly stimulated by the ERK pathway (Haworth et al., 2003). The sustained intracellular acidosis stimulated the NHE1 activity in both wild-type and $PPAR\gamma^{-/-}$ cells (Figure 5A). This stimulation was totally suppressed by PD98059 (Figure 5B), indicating that the ERK-mediated NHE1 stimulation is intact in both cell types. On the other hand, 0.3 μM PGZ rapidly stimulated the NHE1 activity in wild-type, but not in $PPAR\gamma^{-/-}$ cells (Figure 5C). In wild-type cells, PD98059, GW9662, and AG1478, but not a transcriptional inhibitor, actinomycin D, suppressed the PGZ-induced stimulation of NHE1 activity (Figure 5D). Furthermore, GW9662 and AG1478 suppressed the PGZ-induced ERK phosphorylation that was detected only in wild-type cells (Figure 5E). RGZ at 0.3 μM also stimulated the NHE1 activity in wild-type cells by 79.9 ± 10.4% ($p < 0.01$, $n = 8$), but not in $PPAR\gamma^{-/-}$ cells. These results confirmed the existence of PPARγ-dependent nongenomic signaling resulting in ERK activation in wild-type EF cells. They also support the previously proposed view that the constitutive activation of Src/ERK pathway is restricted to mouse PTs and is not found in other mouse tissues such as EF cells (Kiley and Chevalier, 2007).

In contrast to the stimulatory effect of submicromolar concentrations of TZDs, 30 μM PGZ inhibited the NHE1 activity in both wild-type (control, 0.048 ± 0.004 pH unit/min versus PGZ, 0.029 ± 0.002 pH unit/min, $p < 0.01$, $n = 7$) and $PPAR\gamma^{-/-}$ cells (control, 0.048 ± 0.004 pH unit/min versus PGZ, 0.028 ± 0.003 pH unit/min, $p < 0.01$, $n = 7$). RGZ at 30 μM also had a similar inhibitory effect on the NHE1 activity in both wild-type and $PPAR\gamma^{-/-}$ cells (Figure S4). Consistent with a previous study (Oliver et al., 2005), these results indicate that higher micromolar concentrations of TZDs inhibit NHE1 independently of PPARγ as a class effect.

Nongenomic Nature of PPARγ-Dependent Rapid Signaling in EF Cells

To examine whether the NHE1 stimulatory activity of PPARγ can be discriminated from the gene transcriptional activity, we performed adenovirus-mediated transfer of mouse PPARγ1 constructs (Figure 6A) into $PPAR\gamma^{-/-}$ cells. As expected, the full-length PPARγ was able to rescue the NHE1 stimulation and ERK phosphorylation by 0.3 μM PGZ (Figures 6B and 6C). More importantly, the ligand-binding domain (LBD) construct, which lacks the entire N-terminal transcription activation function domain AF-1 and the DNA-binding domain, also rescued the NHE1 stimulation and ERK phosphorylation by 0.3 μM PGZ (Figures 6D and 6E). However, the binding-deficient LBD mutant Q284P, corresponding to human Q286P (Sarraf et al., 1999), failed to rescue the NHE1 stimulation or the ERK phosphorylation (Figures 6D and 6E). The failure of Q284P to rescue the PGZ-mediated

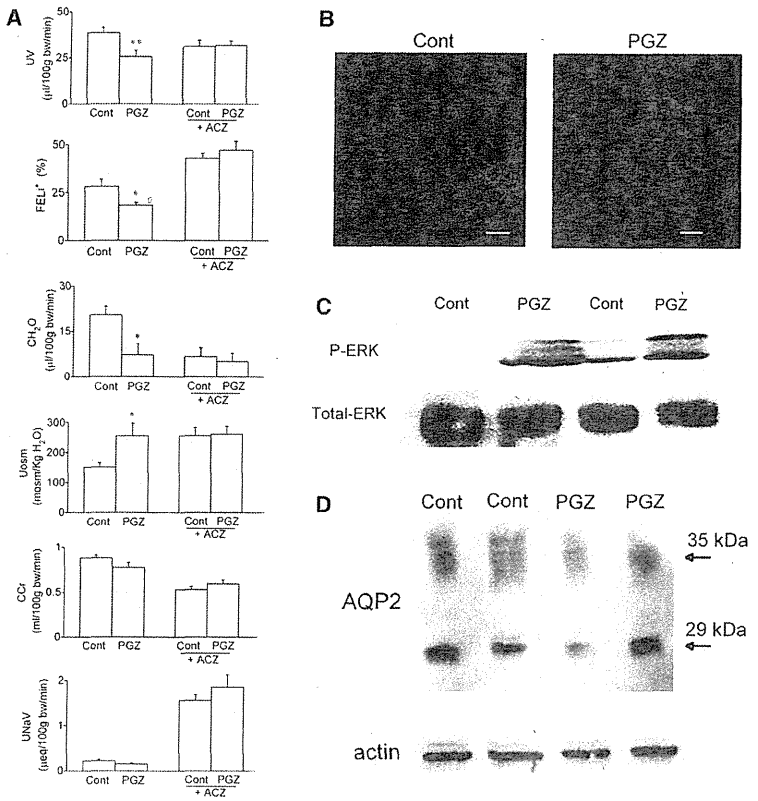

Figure 4. Effects of PGZ on In Vivo PT Transport in Rats

(A) Acute renal clearance study. Urine was collected for 90 min after a single oral dose of 10 mg/kg PGZ or vehicle. *$p < 0.05$ versus control; **$p < 0.01$ versus control. Data are means ± SEM of 11–12 experiments. Each $n = 7$.

(B) Effects of PGZ on ERK phosphorylation in rat kidneys in vivo. Sixty minutes after vehicle (Cont) or PGZ administration, kidneys were removed. Immunohistochemical analysis was performed with the antiphospho-ERK antibody. Green shows phosphorylated ERK, red shows actin, and blue shows nuclei. Bars = 50 μm.

(C) Western blot analysis on rat kidney cortex with the anti-total ERK or the antiphosphorylated ERK antibody. Sixty minutes after vehicle (Cont) or PGZ administration, kidneys were removed. Each lane contained 20 μg of proteins.

(D) Western blot analysis on rat kidney medulla with the anti-AQP2 or the anti-actin antibody. Details are as in (C). See also Figure S3.

NHE1 stimulation was not due to the altered intracellular expression, because the full-length PPARγ, LBD, and Q284P showed an indistinguishable diffuse intracellular expression (Figure 6F). These results indicate that the NHE1 stimulatory activity requires the ligand-binding ability, but not the transcriptional activity, of PPARγ. We confirmed that a 5 min incubation with PGZ did not change the pattern and level of intracellular PPARγ expression.

To further confirm the dissociation of PPARγ-mediated rapid signaling from gene transcription, we examined adipocyte differentiation, which absolutely requires the transcriptional activity of PPARγ (Kubota et al., 1999; Tontonoz et al., 1994). The measurement of triglyceride (TG) contents revealed that wild-type, but not $PPAR\gamma^{-/-}$ cells had adipocyte differentiation ability (Figure S5). Whereas the full-length PPARγ restored the ability of $PPAR\gamma^{-/-}$ cells to differentiate into adipocytes as reported (Kubota et al., 1999), LBD or Q284P failed to restore adipocyte differentiation (Figure S7). These results confirm that the PPARγ-mediated rapid signaling can be dissociated from the gene transcriptional activity.

Roles of Src in PPARγ-Dependent Rapid Signaling in EF Cells

To examine the roles of Src in TZD-induced stimulation of NHE1 activity, we next examined the effects of TZDs in EF cells derived from $Src^{-/-}$ mice (Klinghoffer et al., 1999). In $Src^{+/+}$ control cells, but not in $Src^{-/-}$ cells, 0.3 μM PGZ stimulated the NHE1 activity (Figure 7A). The PGZ-induced ERK phosphorylation was also detected only in $Src^{+/+}$ cells (Figure 7B), though the definite expression of PPARγ was detected in both cell types (Figure 7C). These results confirm that Src is indispensable in PPARγ-dependent nongenomic signaling.

In ER-mediated nongenomic signaling, the association between ER and Src was thought to play a key role (Li et al., 2007). Accordingly, we finally examined a possible interaction between PPARγ and Src by coimmunoprecipitation assay. $PPAR\gamma^{-/-}$ cells were transfected with PPARγ, and cell lysates were subjected to immunoprecipitation with anti-Src or anti-PPARγ antibodies. We found that Src and PPARγ coimmunoprecipitated each other and PGZ markedly enhanced this association (Figures 7D and 7E). PGZ also markedly stimulated the association between Src and LBD (Figure 7F). However, PGZ failed to enhance the association between Src and Q284P, indicating that the TZD-mediated recruitment of Src is dependent on the ligand-binding ability of PPARγ.

DISCUSSION

In the present study we showed that TZDs markedly stimulated sodium-coupled bicarbonate absorption from isolated rabbit, rat, and human PTs by activating both NBCe1 and NHE3 through the PPARγ/Src/EGFR/ERK pathway. Acute PGZ administration in rats induced the stimulation of in vivo PT transport. However, TZDs failed to stimulate in vitro and in vivo PT transport in mice, in which Src-EGFR-ERK is uniquely activated in a constitutive manner. Studies with EF cells confirmed the presence of a nongenomic signaling pathway depending on PPARγ-Src-EGFR-ERK. Because the magnitude of enhancement in PT transport by TZDs was actually comparable to or even exceeded that by angiotensin II (Li et al., 2008), a hormone with the greatest stimulatory effect in this segment, we propose that the stimulation of renal PT transport through PPARγ-dependent nongenomic signaling is involved, at least

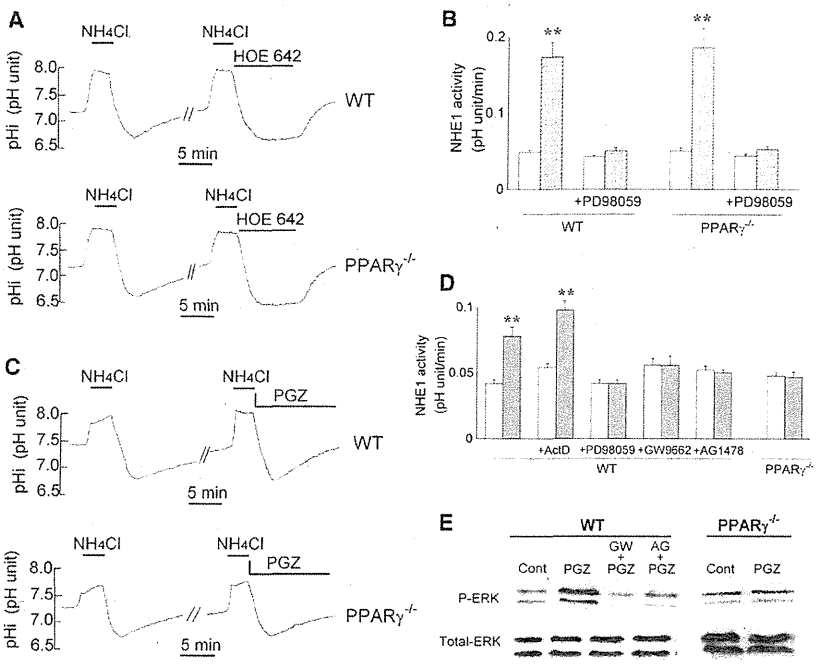

Figure 5. Effects of PGZ on NHE1 Activity in EF Cells

(A) The sustained intracellular acidosis induced by 3 μM HOE642 stimulated the NHE1 activity in both wild-type (WT) and PPARγ$^{-/-}$ cells.

(B) The ERK-dependent activation of NHE1 by sustained intracellular acidosis in EF cells. The NHE1 activity was estimated by the rate of pH_i recovery at pH_i of 6.9. Open bars represent the control activities and hatched bars represent the activities after intracellular acidosis. **$p < 0.01$ versus control. Data are means ± SEM. Each n = 6.

(C) Stimulation of NHE1 activity by 0.3 μM PGZ in wild-type, but not in PPARγ$^{-/-}$ cells.

(D) Signaling mechanism underlying the stimulation of NHE1 activity by PGZ. Actinomycin D (ActD, 5 μM) was added to the medium for 1.5 hr prior to pH_i measurements. Open bars represent the control activities and closed bars represent the activities in the presence of 0.3 μM PGZ. **$p < 0.01$ versus control. Data are means ± SEM of six to seven experiments.

(E) ERK phosphorylation in EF cells. Cells were incubated in the absence or presence of inhibitors for 40 min and 0.3 μM PGZ was added for 5 min. GW; GW9662. AG; AG1478. See also Figure S4.

partially, in TZD-induced volume expansion. Interestingly, the Src-dependent Na/K pump activation by ouabain is dependent on the NHE1 activation (Holthouser et al., 2010). It remains to be determined whether the NHE1 activation plays a similar role in the stimulation of PT transport by TZDs.

Although TZDs are known to trigger diverse rapid cellular signaling events including the activation of kinase signaling pathways such as phosphatidylinositol 3-kinase (PI3K)/Akt, ERK, EGFR transactivation, the production of reactive oxygen species, or Ca^{2+} influx (Burgermeister and Seger, 2008), the mechanisms underlying such dose-, time-, and cell type-dependent responses have been largely unknown. The kinetics of responses, the absolute requirement of ligand-binding ability, and the nonrequirement of transcriptional activity shown in this study clearly indicate that PPARγ, like another nuclear receptor ER (Kousteni et al., 2001), can activate the ERK pathway through the nongenomic mechanism. The dependence on Src, the association between PPARγ and Src, and the negative effect of constitutive Src activation all support the central role of Src in the PPARγ-dependent nongenomic signaling. Src was previously shown to play a similar essential role in the ER-mediated nongenomic signaling (Li et al., 2007). Subpopulations of ER and/or a truncated variant of ER localized to specialized membrane rafts caveolae are associated with several signaling molecules, including Src and eNOS (Li et al., 2003). Interestingly, PPARγ is also associated with caveolin-1 (Burgermeister et al., 2003), raising the possibility that a subset of PPARγ, together with other scaffold and signaling molecules including Src, may form a membrane-localized signaling complex that is responsible for the nongenomic actions. Also, it could be possible that the direct association of PPARγ and MEK (Burgermeister and Seger, 2008) is involved in this signaling complex.

In contrast to the PPARγ-dependent stimulatory effects of submicromolar concentrations of TZDs, suprapharmacological concentrations of TZDs inhibited the NHE1 activity independently of PPARγ. Higher micromolar concentrations of TZDs were known to induce other cellular responses including capacitive calcium entry or rapid cellular acidosis, and such drastic changes in cellular homeostasis could even result in PPARγ-independent ERK activation (Dewar et al., 2007; Friday et al., 2007). Thus, caution is required when acute in vitro responses to higher micromolar concentrations of TZDs are to be analyzed in the absence of ambient proteins. Notably, the protein-unbound peak plasma concentrations of TZDs in human subjects are estimated to be at submicromolar levels (Deng et al., 2005; Krieter et al., 1994), well within the stimulatory range for PT transport.

Our study confirmed that important species differences exist in the mechanism of TZD-induced fluid retention. The studies on collecting duct-specific PPARγ-deficient mice indicate that the distal nephrons play a central role in TZD-induced volume expansion in mice (Guan et al., 2005; Zhang et al., 2005). While the role of ENaC is recently called into question, TZDs may enhance the expression of other sodium and fluid transporters through the classical genomic action of PPARγ (Vallon et al., 2009). The lack of TZD-induced transport stimulation in mice PTs shown in the present study also supports the central role of distal nephrons in TZD-induced volume expansion in mice, though the actual transporter responsible for the enhanced reabsorption in distal nephrons still remains to be determined. On the other hand, several lines of evidence suggest that the transport stimulation in distal nephrons alone cannot explain TZD-induced volume expansion in species other than mice. For example, amiloride failed to prevent the PPARγ agonist-induced volume expansion in rats (Chen et al., 2005).

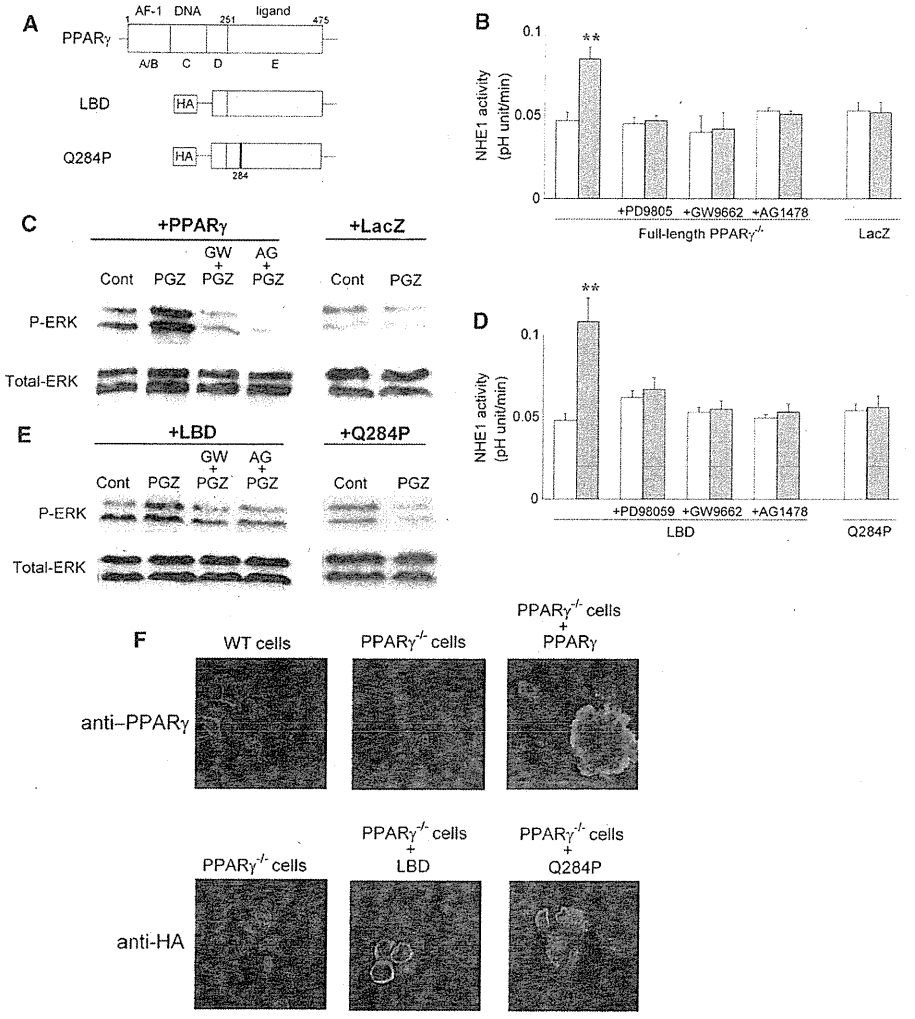

Figure 6. Effects of Adenovirus-Mediated Transfer of PPARγ Constructs into PPARγ$^{-/-}$ Cells

(A) PPARγ constructs. AF-1, transcription activation function domain; DNA, DNA-binding domain; ligand, ligand-binding domain; HA, hemagglutinin.

(B) Full-length PPARγ rescued the PGZ-mediated stimulation of NHE1 activity. Open bars represent the control activities and closed bars represent the activities in the presence of 0.3 μM PGZ. **p < 0.01 versus control. Data are means ± SEM of six to seven experiments.

(C) Full-length PPARγ, but not LacZ, rescued the PGZ-mediated ERK phosphorylation.

(D) LBD, but not Q284P, rescued the PGZ-mediated stimulation of NHE1 activity. Open bars represent the control activities and closed bars represent the activities in the presence of 0.3 μM PGZ. **p < 0.01 versus control. Data are means ± SEM of six to seven experiments.

(E) LBD, but not Q284P, rescued the PGZ-mediated ERK phosphorylation.

(F) Expression of endogenous PPARγ or PPARγ constructs in EF cells. Immunohistochemical analysis was performed by using the anti-PPARγ antibody or the anti-HA antibody. Green shows PPARγ or LBD constructs, red shows actin, and blue shows nuclei. See also Figure S5.

In addition, the chronic administration of TZDs in rats was reported to enhance the renal abundance of α1 subunit of Na^+/K^+ ATPase and the apical Na^+/H^+ exchanger NHE3 in PTs (Song et al., 2004). TZDs were also found to enhance the expression of NHE3 through SGK1-mediated transcriptional activity of PPARγ in cultured human PT cells (Saad et al., 2009). These changes in transporter abundance may further amplify the TZD-induced nongenomic stimulation of PT transport in species other than mice. Consistent with this view, the reduction in lithium clearance was indeed reported in human subjects treated with TZDs (Zanchi et al., 2004). Diuretics targeting the distal nephrons were at least partially effective in preventing TZD-induced mild volume expansion in human subjects with type 2 diabetes (Karalliedde et al., 2006). However, massive volume expansion, the clinically more important side effect sometimes observed in human subjects taking TZDs, is known to be resistant to the conventional diuretic monotherapy (Mudaliar et al., 2003). These considerations support a view that a mechanism other than the stimulation of distal nephron transport is also involved in TZD-induced fluid retention in humans.

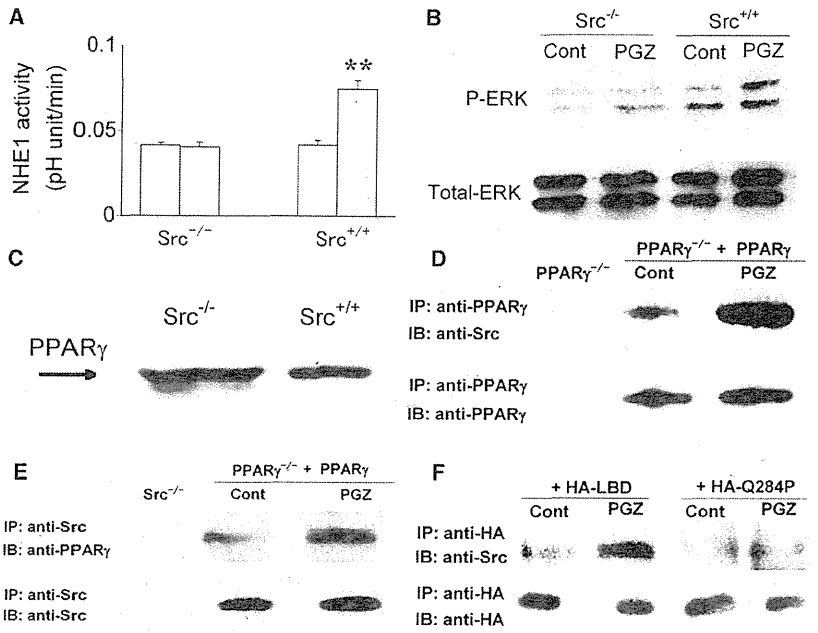

Figure 7. Roles of Src in TZD-Induced Rapid Signaling in EF Cells

(A) Effects of PGZ on NHE1 activity in $Src^{-/-}$ and $Src^{+/+}$ cells. Open bars represent the control activities and closed bars represent the activities in the presence of 0.3 μM PGZ. **$p < 0.01$ versus control. Data are means ± SEM. Each $n = 6$.

(B) PGZ stimulated ERK phosphorylation in $Src^{+/+}$ cells, but not in $Src^{-/-}$ cells. PGZ (0.3 μM) was added for 5 min.

(C) Western blot analysis was performed by using the anti-PPARγ antibody in $Src^{-/-}$ and $Src^{+/+}$ cells.

(D) Immunoprecipitation with the anti-PPARγ antibody in $PPAR\gamma^{-/-}$ cells without or with PPARγ transfection.

(E) Immunoprecipitation with the anti-Src antibody in $Src^{-/-}$ cells (left) or $PPAR\gamma^{-/-}$ cells transfected with PPARγ (middle and right). PGZ (0.3 μM) was added for 5 min.

(F) Immunoprecipitation with the anti-HA antibody in $PPAR\gamma^{-/-}$ cells transfected with LBD or Q284P. PGZ (0.3 μM) was added for 5 min.

In this context, it is noteworthy that the stimulation of sodium transport in distal nephrons alone, induced by excessive aldosterone actions, usually does not result in massive volume expansion with edema formation, because a process known as the "escape phenomenon" suppresses the sodium reabsorption along PTs and other nephron segments (Gonzalez-Campoy et al., 1989). On the other hand, the simultaneous stimulation of sodium transport in PTs and distal nephrons through distinct mechanisms is expected, at least under certain conditions, to operate in a synergic manner. Massive volume expansion in human subjects usually occurs after weeks of use of TZDs. However, it can also occur as rapidly as 4 days after use of TZDs (Hirsch et al., 1999), supporting the involvement of multiple mechanisms. Thus, combination therapy with different diuretics targeting both PTs and the distal nephrons could be a therapeutic option in case of TZD-induced massive volume expansion.

Finally, this study represents an alternative paradigm in the emerging concept that nuclear hormone receptors can mediate nongenomic actions (Lösel and Wehling, 2003). Different ligands can bind to LBD of PPARγ in slightly different ways and induce different biological responses (Zhang et al., 2007). It could be possible, therefore, to discriminate the diverse PPARγ actions at least partially by modifying the ligand-induced conformational changes. Indeed, several selective PPARγ modulators developed by such a concept are known to induce less fluid retention at least in animals (Higgins and Depaoli, 2010). Future studies are required to determine whether these selective PPARγ modulators can also prevent massive fluid retention in humans.

EXPERIMENTAL PROCEDURES

Measurements of NBCe1 and NHE3 Activities in Renal Proximal Tubules

All animal procedures were in accordance with local institutional guidelines. Japanese white rabbits, Wistar rats, or C57BL/6 mice were sacrificed with excessive amounts of pentobarbital and thin slices of kidney cortex were obtained. For human PTs, kidney cortex tissues were obtained during the unilateral nephrectomy for renal carcinoma. The institutional review board of University of Tokyo School of Medicine approved the study and written informed consent was obtained from all the subjects. The PT (S2 segment) fragment was microdissected manually and transferred to a perfusion chamber mounted on an inverted microscope. For the analysis of NBCe1 activity, the luminally collapsed tubule was used as described (Li et al., 2008). The tubule was incubated with an acetoxymethyl ester form of a pH-sensitive fluorescence dye 2′,7′-bis(carboxyethyl)-5(6)-carboxyfluorescein (BCECF/AM; Dojindo) and pH_i was monitored with a photometry system (OSP-10; Olympus). Calibration curves for pH_i were obtained according to the method described (Thomas et al., 1979). Prewarmed (38°C) Dulbecco's modified Eagle's medium (DMEM) equilibrated with 5% CO_2/95% O_2 gas was used for the peritubular perfusate, which was shown to be essential for the long-term functional preservation of isolated PTs (Müller-Berger et al., 1997; Zheng et al., 2003) The rate of pH_i decrease to bath HCO_3^- reduction and the buffer capacity were used to calculate the NBCe1 activity as described (Li et al., 2008). For the analysis of NHE3 activity, pH_i was monitored in the microperfused S2 segment as described (Yamada et al., 1996). Initially, both luminal and bath sides were perfused with HEPES-buffered Ringer solution equilibrated with 100% O_2 and thereafter, luminal perfusate was switched to Na^+-free HEPES solution that replaces Na^+ in HEPES-buffered Ringer solution with N-methyl-D-glucamine. The resultant decrease in pH_i was shown to reflect the luminal NHE3 activity (Yamada et al., 1996).

Determination of Bicarbonate Absorption Rates

We used the stop-flow microspectrofluorometric method as described (Müller-Berger et al., 1999; Zheng et al., 2003). Isolated PTs were microperfused and luminal pH (pH_L) was monitored on the OSP-10 system. The tubular lumen was perfused with Ringer solution, which contained 25 mM HCO_3^-, 40 mM raffinose, and 40 mM BCECF, and DMEM was used for the bath perfusate. To determine $JHCO_3^-$, we abruptly stopped the rapid (~80 nl/min) luminal perfusion by suddenly reducing the perfusion pressure from ~18 to 0 cm H_2O. The decay in luminal HCO_3^- concentration was calculated from the changes in pH_L and $JHCO_3^-$ was calculated as described (Müller-Berger et al., 1999).

Renal Clearance Protocol

Adult female Wistar rats weighing between 140 and 170 g were used. The rats were individually housed in metabolic cages. Three days before study, the diet

was changed from a standard diet to one containing lithium chloride (6 mM/kg dry weight) to yield measurable plasma lithium concentrations without affecting renal function (Shalmi and Thomsen, 1989). On the morning of clearance study water and food were withdrawn and maximal diuresis was induced by water loading to facilitate the detection of rapid alterations in PT transport. Each rat received a load of tap water by gavage (5% of the body weight), followed by a second load of the same volume with PGZ (n = 12) or vehicle (citric acid, n = 12) 4 hr later. Thirty minutes after the second load, spontaneously voided urine was collected over 90 min. In the ACZ group, ACZ (100 mg/kg BW) was given orally with PGZ (n = 11) or the vehicle (n = 12). At the end of the experiment, blood samples were drawn through cardiac puncture in anesthetized rats. Serum and urine data were measured by the SRL clinical service. Renal clearance (C) was calculated by a standard formula (C = UV/P) and CH_2O was calculated by the following formula: CH_2O = (1 − Uosm/Posm) × UV, where Uosm and Posm denote osmolality of urine and plasma, respectively. $FELi^+$ was calculated as CLi^+/CCr. The blood pressure of restrained conscious rats was measured by a programmed tail-cuff sphygmomanometer (BP-98A; Softron).

Measurement of NHE1 Activity

EF cells from wild-type and $PPAR\gamma^{-/-}$ mice were harvested from 13.5 dpc embryos and were maintained in DMEM supplemented with 10% fetal bovine serum (FBS) as described (Klinghoffer et al., 1999). EF cells derived from mouse embryos deficient in c-Src, Yes, and Fyn ($Src^{-/-}$) or from embryos lacking both Yes and Fyn, but maintaining normal levels of c-Src ($Src^{+/+}$), were obtained from American Type Culture Collection. When cells reached confluency, they were trypsinized and seeded onto 6 mm round coverslips. Cell-coated coverslips were incubated with HEPES-buffered Ringer solution containing BCECF/AM for 30–60 min at room temperature. The coverslip was then superfused with prewarmed (38°C) experimental solutions at ~5 ml/min. The NHE1 activity was determined as described (Haworth et al., 2003). Briefly, the HEPES solution was changed to another solution containing 20 mM NH_4Cl (instead of the equimolar NaCl) for several minutes. The reintroduction of the HEPES solution typically induced pH_i to decrease to a level around pH 6.7 and thereafter, pH_i started to recover from intracellular acidosis. This pH_i recovery reflects the NHE1 activity, because it was almost completely inhibited by 3 μM HOE642 (Sanofi Aventis), a specific inhibitor of NHE1. The NHE1 activity was estimated by calculating the rate of pH_i recovery at fixed pH_i of 6.9 during the recovery from intracellular acidosis.

Adenovirus-Mediated Gene Transfer

The full-length mouse PPARγ1 expression vector for adenovirus-mediated gene transfer was constructed by using AdEasy Vector system (Promega) and pCMX-PPARγ1 (kindly provided by Dr. B. M. Spiegelman) according to the manufacturer's instructions. In addition, the hemagglutinin (HA)-tagged LBD of PPARγ, corresponding to amino acids 184–475, and the LBD containing Q284P mutation, which is devoid of the binding affinity for TZDs (Sarraf et al., 1999), were constructed by PCR-based site-directed mutagenesis (Stratagene) and confirmed by DNA sequencing. These constructs were also subcloned into the adenovirus vector. The EF cells were infected with each recombinant virus at a multiplicity of infection of 220 plaque-forming units/cell, and 48 hr later pH_i measurement was performed.

Antibodies

The anti-PPARγ antibodies were from Santa Cruz Biotechnology, the rabbit anti-HA was from Bethyl Laboratories, and the rabbit and mouse anti-Src were from Cell Signaling Technology. Antibodies against total ERK, phospho-ERK (P-ERK), nonphospho-Src (NP-Src), and phospho-Src (P-Src, tyrosine-416) were from Cell Signaling Technology. The horseradish peroxidase (HRP)-conjugated anti-rabbit or anti-mouse IgG were from Jackson ImmunoResearch Laboratories. Alexa Fluor 488 anti-rabbit IgG and Alexa Fluor 568 phalloidin were from Molecular Probes and 4′,6-diamidino-2-phenylindole dihydrochloride (DAPI) was from Boehringer Mannheim.

Immunoblotting and Immunoprecipitation

For detection of PPARγ, kidney tissues or cell samples were homogenized in ice-cold buffer containing 280 mmol/L sucrose and complete protease inhibitor cocktail (Roche). For detection of PPARγ in PTs, human PTs of ~1 mm length were manually dissected from thin kidney slices and were homogenized in the same buffer. For detection of phosphorylation of ERK or Src, thin slices of kidney cortex were obtained. They were divided into pieces of small bundles consisting mostly of PTs as described (Li et al., 2008). These samples were incubated at 37°C for 40 min in DMEM under 5% CO_2 in the absence or presence of several inhibitors. After TZDs were added for the indicated time, samples were homogenized in ice-cold lysis buffer containing 25 mM Tris-HCl (pH 7.4), 10 mM sodium orthovanadate, 10 mM sodium pyrophosphate, 100 mM sodium fluoride, 10 mM EDTA, 10 mM EGTA, and 1 mM phenylmethylsulfonyl fluoride. For detection of in vivo ERK phosphorylation, rats were sacrificed with excessive amounts of pentobarbital and kidney cortex samples were immediately homogenized in the lysis buffer. Equal amounts of protein samples were obtained from the supernatants, separated by SDS-PAGE on 7% acrylamide minigels, and transferred to a nitrocellulose membrane. After incubation in blocking buffer, the membrane was treated with one of the primary antibodies and then with their respective secondary antibodies. The signal was detected by an ECL Plus system (Amersham).

EF cells were grown on a 10 cm culture dish and FBS was removed overnight. Thereafter, cells were incubated for 40 min in the absence and presence of several inhibitors. After TZDs were added for the indicated time, cells were collected, lysed with the lysis buffer, and subjected to immunoblotting. For immunoprecipitation with PPARγ or Src, the cell lysate was precleaned by incubation with Protein G Sepharose 4 Fast Flow (GE Healthcare Bio-Science) and incubated with the mouse anti-PPARγ or the mouse anti-Src antibodies coupled to Protein G Sepharose 4 Fast Flow. The immunoprecipitates were washed three to five times with the lysis buffer containing 1% Nonidet P-40 and subjected to immunoblotting with the rabbit anti-PPARγ or the rabbit anti-Src antibody. For immunoprecipitation with HA, the rabbit anti-HA antibody was coupled to Protein A Sepharose 4 Fast Flow (GE Healthcare Bio-Science) and immunoblotting was performed with the rabbit anti-HA or the rabbit anti-Src antibody.

Immunohistochemical Analysis

To examine the intrarenal expression of PPARγ, we fixed the kidney samples from humans and rabbits with buffered 4% paraformaldehyde (PFA), sectioned them 5 μm thick in the cryostat at −25°C, air-dried them, and immersed them in PBS, which was followed by incubation with anti-PPARγ (1:100 dilution) overnight at 4°C. The specimens were subsequently incubated with the mixtures of Alexa Fluor 488 anti-rabbit or anti-goat IgG, Alexa Fluor 568 phalloidin for labeling of F-actin, and DAPI for labeling of nuclei for 60 min at room temperature. The kidneys from rats and mice were frozen without fixation and cryosectioned at 10 μm thick and then fixed with buffered 4% PFA for 10 min. After being washed with PBS, sections were serially incubated with anti-PPARγ (1:50) for 1 hr and the mixtures of Cy5-conjugated anti-rabbit IgG, Alexa Fluor 568 phalloidin, and SYBR Green I for nuclei for 30 min at room temperature. An absorption test was performed in the presence of antigen peptide (10 mg/L). The specimens were observed with a confocal laser scanning microscope (MRC-1024K; Japan Bio-Rad Laboratories or LSM510META, Carl Zeiss). For the determination of intrarenal ERK phosphorylation, the antiphospho-ERK and Alexa Fluor 488 anti-rabbit IgG were used. To examine the expression of endogenous PPARγ or exogenous PPARγ constructs in EF cells, we fixed the cells with buffered 4% PFA and processed them for immunostaining as described above by using the anti-PPARγ antibody or the anti-HA antibody as the primary antibody.

Adipocyte Differentiation

EF cells were plated on six-well plastic dishes and propagated to confluence. Two days later, medium was replaced with standard differentiation medium containing 0.5 mM 3-isobutyl-1-methylxanthine, 10 μM dexamethasone, 0.86 μM insulin, 0.3 μM PGZ, and 10% FBS. After 8 days, cells were harvested. The TG levels in the cell lysates were quantified by using the Triglyceride E-test Wako kit (Wako Pure Chemical) according to the manufacturer's protocol.

Statistical Analysis

Data are means ± SEM. Significant differences were determined by applying Student's t test or ANOVA with Bonferroni's adjustment as appropriate. Statistical significance was set at $p < 0.05$.

SUPPLEMENTAL INFORMATION

Supplemental Information includes five figures and can be found with this article online at doi:10.1016/j.cmet.2011.02.015.

ACKNOWLEDGMENTS

This study was supported in part by grants from the Ministry of Education, Culture, Sports, Science and Technology of Japan and in part by a grant from Takeda Pharmaceutical Co., Ltd. The authors thank Ms. Tomoko Miura (Department of Anatomy, Kyorin University School of Medicine) for technical assistance.

Received: September 14, 2010
Revised: January 10, 2011
Accepted: February 17, 2011
Published: May 3, 2011

REFERENCES

Burgermeister, E., and Seger, R. (2008). PPARgamma and MEK interactions in cancer. PPAR Res. *2008*, 309469.

Burgermeister, E., Tencer, L., and Liscovitch, M. (2003). Peroxisome proliferator-activated receptor-γ upregulates caveolin-1 and caveolin-2 expression in human carcinoma cells. Oncogene *22*, 3888–3900.

Chen, L., Yang, B., McNulty, J.A., Clifton, L.G., Binz, J.G., Grimes, A.M., Strum, J.C., Harrington, W.W., Chen, Z., Balon, T.W., et al. (2005). GI262570, a peroxisome proliferator-activated receptor γ agonist, changes electrolytes and water reabsorption from the distal nephron in rats. J. Pharmacol. Exp. Ther. *312*, 718–725.

de Rouffignac, C., Elalouf, J.M., and Roinel, N. (1991). Glucagon inhibits water and NaCl transports in the proximal convoluted tubule of the rat kidney. Pflugers Arch. *419*, 472–477.

Deng, L.J., Wang, F., and Li, H.D. (2005). Effect of gemfibrozil on the pharmacokinetics of pioglitazone. Eur. J. Clin. Pharmacol. *61*, 831–836.

Dewar, B.J., Gardner, O.S., Chen, C.S., Earp, H.S., Samet, J.M., and Graves, L.M. (2007). Capacitative calcium entry contributes to the differential transactivation of the epidermal growth factor receptor in response to thiazolidinediones. Mol. Pharmacol. *72*, 1146–1156.

Friday, E., Oliver, R., 3rd, Welbourne, T., and Turturro, F. (2007). Role of epidermal growth factor receptor (EGFR)-signaling versus cellular acidosis via Na^+/H^+ exchanger1(NHE1)-inhibition in troglitazone-induced growth arrest of breast cancer-derived cells MCF-7. Cell. Physiol. Biochem. *20*, 751–762.

Gonzalez-Campoy, J.M., Romero, J.C., and Knox, F.G. (1989). Escape from the sodium-retaining effects of mineralocorticoids: role of ANF and intrarenal hormone systems. Kidney Int. *35*, 767–777.

Guan, Y., Zhang, Y., Davis, L., and Breyer, M.D. (1997). Expression of peroxisome proliferator-activated receptors in urinary tract of rabbits and humans. Am. J. Physiol. *273*, F1013–F1022.

Guan, Y., Hao, C., Cha, D.R., Rao, R., Lu, W., Kohan, D.E., Magnuson, M.A., Redha, R., Zhang, Y., and Breyer, M.D. (2005). Thiazolidinediones expand body fluid volume through PPARgamma stimulation of ENaC-mediated renal salt absorption. Nat. Med. *11*, 861–866.

Haworth, R.S., McCann, C., Snabaitis, A.K., Roberts, N.A., and Avkiran, M. (2003). Stimulation of the plasma membrane Na^+/H^+ exchanger NHE1 by sustained intracellular acidosis. Evidence for a novel mechanism mediated by the ERK pathway. J. Biol. Chem. *278*, 31676–31684.

Higgins, L.S., and Depaoli, A.M. (2010). Selective peroxisome proliferator-activated receptor γ (PPARgamma) modulation as a strategy for safer therapeutic PPARgamma activation. Am. J. Clin. Nutr. *91*, 267S–272S.

Hirsch, I.B., Kelly, J., and Cooper, S. (1999). Pulmonary edema associated with troglitazone therapy. Arch. Intern. Med. *159*, 1811.

Holthouser, K.A., Mandal, A., Merchant, M.L., Schelling, J.R., Delamere, N.A., Valdes, R.R., Jr., Tyagi, S.C., Lederer, E.D., and Khundmiri, S.J. (2010). Ouabain stimulates Na-K-ATPase through a sodium/hydrogen exchanger-1 (NHE-1)-dependent mechanism in human kidney proximal tubule cells. Am. J. Physiol. Renal Physiol. *299*, F77–F90.

Hong, G., Lockhart, A., Davis, B., Rahmoune, H., Baker, S., Ye, L., Thompson, P., Shou, Y., O'Shaughnessy, K., Ronco, P., and Brown, J. (2003). PPARgamma activation enhances cell surface ENaCalpha via up-regulation of SGK1 in human collecting duct cells. FASEB J. *17*, 1966–1968.

Karalliedde, J., Buckingham, R., Starkie, M., Lorand, D., Stewart, M., and Viberti, G.; Rosiglitazone Fluid Retention Study Group. (2006). Effect of various diuretic treatments on rosiglitazone-induced fluid retention. J. Am. Soc. Nephrol. *17*, 3482–3490.

Kiley, S.C., and Chevalier, R.L. (2007). Species differences in renal Src activity direct EGF receptor regulation in life or death response to EGF. Am. J. Physiol. Renal Physiol. *293*, F895–F903.

Klinghoffer, R.A., Sachsenmaier, C., Cooper, J.A., and Soriano, P. (1999). Src family kinases are required for integrin but not PDGFR signal transduction. EMBO J. *18*, 2459–2471.

Kousteni, S., Bellido, T., Plotkin, L.I., O'Brien, C.A., Bodenner, D.L., Han, L., Han, K., DiGregorio, G.B., Katzenellenbogen, J.A., Katzenellenbogen, B.S., et al. (2001). Nongenotropic, sex-nonspecific signaling through the estrogen or androgen receptors: dissociation from transcriptional activity. Cell *104*, 719–730.

Krieter, P.A., Colletti, A.E., Doss, G.A., and Miller, R.R. (1994). Disposition and metabolism of the hypoglycemic agent pioglitazone in rats. Drug Metab. Dispos. *22*, 625–630.

Kubota, N., Terauchi, Y., Miki, H., Tamemoto, H., Yamauchi, T., Komeda, K., Satoh, S., Nakano, R., Ishii, C., Sugiyama, T., et al. (1999). PPAR γ mediates high-fat diet-induced adipocyte hypertrophy and insulin resistance. Mol. Cell *4*, 597–609.

Li, L., Haynes, M.P., and Bender, J.R. (2003). Plasma membrane localization and function of the estrogen receptor alpha variant (ER46) in human endothelial cells. Proc. Natl. Acad. Sci. USA *100*, 4807–4812.

Li, L., Hisamoto, K., Kim, K.H., Haynes, M.P., Bauer, P.M., Sanjay, A., Collinge, M., Baron, R., Sessa, W.C., and Bender, J.R. (2007). Variant estrogen receptor-c-Src molecular interdependence and c-Src structural requirements for endothelial NO synthase activation. Proc. Natl. Acad. Sci. USA *104*, 16468–16473.

Li, Y., Yamada, H., Kita, Y., Kunimi, M., Horita, S., Suzuki, M., Endo, Y., Shimizu, T., Seki, G., and Fujita, T. (2008). Roles of ERK and cPLA2 in the angiotensin II-mediated biphasic regulation of Na^+-HCO_3^- transport. J. Am. Soc. Nephrol. *19*, 252–259.

Lösel, R., and Wehling, M. (2003). Nongenomic actions of steroid hormones. Nat. Rev. Mol. Cell Biol. *4*, 46–56.

Mudaliar, S., Chang, A.R., and Henry, R.R. (2003). Thiazolidinediones, peripheral edema, and type 2 diabetes: incidence, pathophysiology, and clinical implications. Endocr. Pract. *9*, 406–416.

Müller-Berger, S., Coppola, S., Samarzija, I., Seki, G., and Frömter, E. (1997). Partial recovery of in vivo function by improved incubation conditions of isolated renal proximal tubule. I. Change of amiloride-inhibitable K^+ conductance. Pflugers Arch. *434*, 373–382.

Müller-Berger, S., Samarzija, I., Kunimi, M., Yamada, H., Frömter, E., and Seki, G. (1999). A stop-flow microperfusion technique for rapid determination of HCO_3^- absorption/H^+ secretion by isolated renal tubules. Pflugers Arch. *439*, 208–215.

Muto, S., Miyata, Y., Imai, M., and Asano, Y. (2001). Troglitazone stimulates basolateral rheogenic Na^+/HCO_3^- cotransport activity in rabbit proximal straight tubules. Exp. Nephrol. *9*, 191–197.

Nofziger, C., Chen, L., Shane, M.A., Smith, C.D., Brown, K.K., and Blazer-Yost, B.L. (2005). PPARgamma agonists do not directly enhance basal or insulin-stimulated Na+ transport via the epithelial Na+ channel. Pflugers Arch. *451*, 445–453.

Oliver, R., 3rd, Friday, E., Turturro, F., Lacy, A., and Welbourne, T. (2005). Troglitazone's rapid and sustained activation of ERK1/2 induces cellular acidosis in LLC-PK1-F^+ cells: physiological responses. Am. J. Physiol. Renal Physiol. *288*, F1257–F1266.

Ryan, M.J., Didion, S.P., Mathur, S., Faraci, F.M., and Sigmund, C.D. (2004). PPARγ agonist rosiglitazone improves vascular function and lowers blood pressure in hypertensive transgenic mice. Hypertension *43*, 661–666.

Saad, S., Agapiou, D.J., Chen, X.M., Stevens, V., and Pollock, C.A. (2009). The role of Sgk-1 in the upregulation of transport proteins by PPAR-γ agonists in human proximal tubule cells. Nephrol. Dial. Transplant. *24*, 1130–1141.

Sarraf, P., Mueller, E., Smith, W.M., Wright, H.M., Kum, J.B., Aaltonen, L.A., de la Chapelle, A., Spiegelman, B.M., and Eng, C. (1999). Loss-of-function mutations in PPAR γ associated with human colon cancer. Mol. Cell *3*, 799–804.

Shalmi, M., and Thomsen, K. (1989). Alterations of lithium clearance in rats by different modes of lithium administration. Ren. Physiol. Biochem. *12*, 273–280.

Song, J., Knepper, M.A., Hu, X., Verbalis, J.G., and Ecelbarger, C.A. (2004). Rosiglitazone activates renal sodium- and water-reabsorptive pathways and lowers blood pressure in normal rats. J. Pharmacol. Exp. Ther. *308*, 426–433.

Thomas, J.A., Buchsbaum, R.N., Zimniak, A., and Racker, E. (1979). Intracellular pH measurements in Ehrlich ascites tumor cells utilizing spectroscopic probes generated in situ. Biochemistry *18*, 2210–2218.

Tontonoz, P., Hu, E., and Spiegelman, B.M. (1994). Stimulation of adipogenesis in fibroblasts by PPARγ2, a lipid-activated transcription factor. Cell *79*, 1147–1156.

Vallon, V., Hummler, E., Rieg, T., Pochynyuk, O., Bugaj, V., Schroth, J., Dechenes, G., Rossier, B., Cunard, R., and Stockand, J. (2009). Thiazolidinedione-induced fluid retention is independent of collecting duct alphaENaC activity. J. Am. Soc. Nephrol. *20*, 721–729.

Yamada, H., Seki, G., Taniguchi, S., Uwatoko, S., Nosaka, K., Suzuki, K., and Kurokawa, K. (1996). Roles of Ca^{2+} and PKC in regulation of acid/base transport in isolated proximal tubules. Am. J. Physiol. *271*, F1068–F1076.

Yki-Järvinen, H. (2004). Thiazolidinediones. N. Engl. J. Med. *351*, 1106–1118.

Zanchi, A., Chiolero, A., Maillard, M., Nussberger, J., Brunner, H.R., and Burnier, M. (2004). Effects of the peroxisomal proliferator-activated receptor-γ agonist pioglitazone on renal and hormonal responses to salt in healthy men. J. Clin. Endocrinol. Metab. *89*, 1140–1145.

Zhang, H., Zhang, A., Kohan, D.E., Nelson, R.D., Gonzalez, F.J., and Yang, T. (2005). Collecting duct-specific deletion of peroxisome proliferator-activated receptor γ blocks thiazolidinedione-induced fluid retention. Proc. Natl. Acad. Sci. USA *102*, 9406–9411.

Zhang, F., Lavan, B.E., and Gregoire, F.M. (2007). Selective modulators of PPAR-gamma activity: molecular aspects related to obesity and side-effects. PPAR Res. *2007*, 32696.

Zheng, Y., Horita, S., Hara, C., Kunimi, M., Yamada, H., Sugaya, T., Goto, A., Fujita, T., and Seki, G. (2003). Biphasic regulation of renal proximal bicarbonate absorption by luminal AT1A receptor. J. Am. Soc. Nephrol. *14*, 1116–1122.

Apoptosis inhibitor of macrophage (AIM) is required for obesity-associated recruitment of inflammatory macrophages into adipose tissue

Jun Kurokawa[a], Hiromichi Nagano[a], Osamu Ohara[b], Naoto Kubota[c], Takashi Kadowaki[c], Satoko Arai[a], and Toru Miyazaki[a,1]

[a]Laboratory of Molecular Biomedicine for Pathogenesis, Center for Disease Biology and Integrative Medicine, Faculty of Medicine, University of Tokyo, Tokyo 113-0033, Japan; [b]Department of Human Genome Research, Kazusa DNA Research Institute, Kisarazu, Chiba 292-0818, Japan; and [c]Department of Internal Medicine, Graduate School of Medicine, University of Tokyo, Tokyo 113-0033, Japan

Edited* by Tadatsugu Taniguchi, University of Tokyo, Tokyo, Japan, and approved June 14, 2011 (received for review February 3, 2011)

Infiltration of inflammatory macrophages into adipose tissues with the progression of obesity triggers insulin resistance and obesity-related metabolic diseases. We recently reported that macrophage-derived apoptosis inhibitor of macrophage (AIM) protein is increased in blood in line with obesity progression and is incorporated into adipocytes, thereby inducing lipolysis in adipose tissue. Here we show that such a response is required for the recruitment of adipose tissue macrophages. In vitro, AIM-dependent lipolysis induced an efflux of palmitic and stearic acids from 3T3-L1 adipocytes, thereby stimulating chemokine production in adipocytes via activation of toll-like receptor 4 (TLR4). In vivo administration of recombinant AIM to *TLR4*-deficient (*TLR4*$^{-/-}$) mice resulted in induction of lipolysis without chemokine production in adipose tissues. Consistently, mRNA levels for the chemokines that affect macrophages were far lower in *AIM*-deficient (*AIM*$^{-/-}$) than in wild-type (*AIM*$^{+/+}$) obese adipose tissue. This reduction in chemokine production resulted in a marked prevention of inflammatory macrophage infiltration into adipose tissue in obese *AIM*$^{-/-}$ mice, although these mice showed more advanced obesity than *AIM*$^{+/+}$ mice on a high-fat diet. Diminished macrophage infiltration resulted in decreased inflammation locally and systemically in obese *AIM*$^{-/-}$ mice, thereby protecting them from insulin resistance and glucose intolerance. These results indicate that the increase in blood AIM is a critical event for the initiation of macrophage recruitment into adipose tissue, which is followed by insulin resistance. Thus, AIM suppression might be therapeutically applicable for the prevention of obesity-related metabolic disorders.

diabetes | fatty acid synthase | CD36 | knockout mouse

Chronic, low-grade inflammation observed in adipose tissues is characteristic of obesity. Such a subclinical inflammatory state of adipose tissues is highly associated with insulin resistance both in adipose tissue and systemically and thus contributes to the development of multiple obesity-induced metabolic and cardiovascular diseases (1–4). Evidence has shown that infiltration of a large number of classically activated inflammatory macrophages (M1 macrophages) into adipose tissue is responsible for obesity-associated inflammation (5–7). Lean adipose tissue contains a resident population of alternatively activated macrophages (M2 macrophages), which can suppress the inflammation of both adipocytes and macrophages partly via the secretion of interleukin (IL)-10. Hence, obesity induces a switch in macrophage activation state in adipose tissue toward M1 polarization, which leads to inflammation (8–12). However, the mechanism that promotes infiltration of inflammatory macrophages into obese adipose tissue is as yet unknown.

We recently reported that the apoptosis inhibitor of macrophage (AIM) protein (13) is incorporated into adipocytes via CD36-mediated endocytosis, and induces lipolysis by suppressing the activity of fatty acid synthase (FAS) (14). AIM is a member of the scavenger receptor cysteine-rich superfamily and was initially identified as an apoptosis inhibitor that supports the survival of macrophages against different types of apoptosis-inducing stimuli (13). AIM is a direct target for regulation by nuclear receptor liver X receptor/retinoid X receptor (LXR/RXR) heterodimers (15, 16) and is solely produced by tissue macrophages. As a secreted molecule, AIM is detected in both human and mouse blood at various levels (13, 16–19) and increases in blood with the progression of obesity in mice fed a high-fat diet (HFD) (14). The augmented blood AIM induced lipolysis, as evident by the fact that the increase of free fatty acids (FFAs) and glycerol in blood was suppressed in *AIM*$^{-/-}$ mice (14). Owing to less lipolysis, adipocyte hypertrophy was more advanced and the overall mass of visceral adipose tissues was greater in *AIM*$^{-/-}$ than in *AIM*$^{+/+}$ mice fed a HFD (14). All these observations imply that AIM-induced lipolysis might be responsible for the obesity-associated recruitment of adipose tissue macrophages.

In the present study, we assessed whether AIM affects macrophage accumulation in adipose tissues in obese mice. In addition, we determined the molecular mechanism of how AIM-dependent lipolysis results in the production of chemokines by adipocytes for the effective recruitment of adipose tissue macrophages. Finally, we investigated how the absence of AIM influences the local and systemic inflammatory state and insulin resistance in mice. On the basis of these results, we discuss the putative role of AIM in the initiation of obesity-associated chronic inflammation and subsequent metabolic diseases.

Results and Discussion

Prevention of M1 Macrophage Recruitment into Adipose Tissues in Obese *AIM*$^{-/-}$ Mice. In *AIM*$^{-/-}$ mice, adipocyte hypertrophy was more advanced than in *AIM*$^{+/+}$ mice, and the overall mass of visceral fat as well as body weight was markedly greater compared with that of *AIM*$^{+/+}$ mice (14). Interestingly, however, far fewer macrophages stained with a pan-macrophage antibody F4/80 were observed in epididymal adipose tissue in *AIM*$^{-/-}$ mice than in *AIM*$^{+/+}$ mice fed a HFD for 12 wk (Fig. 1*A*). The number of IL-6 stained inflammatory type (M1) macrophages in obese *AIM*$^{-/-}$ mice was markedly lower than in obese *AIM*$^{+/+}$ mice (Fig. 1*A*). In addition, almost no M1 macrophage clusters forming crown-like structures (CLS) were observed in obese *AIM*$^{-/-}$ mice (Fig. 1*A*). In contrast, the number of M2 adipose tissue macrophages stained for mannose receptor (MR) was not increased in *AIM*$^{+/+}$ or *AIM*$^{-/-}$ mice after a 12-wk HFD (Fig. 1*B*). Furthermore, the stromal-vascular cell fraction (SVF) containing macrophages was isolated from the epididymal fat tissue of lean and obese mice by collagenase treatment and

Author contributions: T.M. designed research; J.K., O.O., N.K., and S.A. performed research; H.N. contributed new reagents/analytic tools; J.K., O.O., T.K., and T.M. analyzed data; and S.A. and T.M. wrote the paper.

The authors declare no conflict of interest.

*This Direct Submission article had a prearranged editor.

[1]To whom correspondence should be addressed. E-mail: tm@m.u-tokyo.ac.jp.

This article contains supporting information online at www.pnas.org/lookup/suppl/doi:10.1073/pnas.1101841108/-/DCSupplemental.